The page and line numbers used in the response are referring to the revised manuscript, which is appended to this response. Note that this is not the final revised manuscript, but is provided to show the reviewers where we made changes to address their concerns.

Anonymous Referee #2

Received and published: 12 December 2019

1 General remarks

The manuscript analyses airborne radiation observations and satellite observations of Arctic clouds. A surface albedo parametrization is derived to account for the inhomogeneous Arctic sea ice surface. Spectral and broadband are compared to radiative transfer simulations which are based on satellite observations. The spectral irradiance is analyzed to untangle uncertainties resulting from the surface albedo and the cloud optical properties.

In general, the analysis of airborne observations in remote Arctic areas is of high value and provides one rare tool to validate satellite observations. Therefore, the study has high potential and is within the scope of AMT. It could have a wide scientific interest and might contribute to improve our understanding of Arctic clouds. However, the manuscript lacks in several major issues and therefore, does not exhaust its full potential. These issues have to be reassessed in detail before publishing the manuscript.

First, the objective of the study is not well presented and outlined. Based on the title and introduction, the readers expectations and the presented analysis may strongly differ. This deficiency might results from a non-existing description of a general approach and methodology how the measurements can and will be used to validate and improve satellite observations. Such a general strategy is an important part of the manuscript in order to promote future application of the methods. Based on the unclear objectives also the conclusions are weak and leave many questions unanswered putting off the reader with promises for future studies. Finally, a throughout uncertainty estimation is missing, which is mandatory if observations are used for validation purposes. I'm sure, there are options to restructure and improve the manuscript in a way that it presents the full potential of the study.

Below, I compiled a list of comments which have to be considered in a revised version of the paper. There might be some contradictory statements which result from my misinterpretation of the text when first reading the manuscript. I am sure the authors will know how to weight in such cases and how to improve the text to avoid misinterpretations by other readers.

R: Thank you very much for your perspective. As we now realize, the manuscript had some serious shortcomings (especially regarding the uncertainty analysis), which we believe we addressed with the revised version. The annotated revised manuscript is attached to this response; page/line numbers refer to that version unless stated otherwise. We do think that we stated the objectives in the original manuscript (p4l16, original manuscript). However, the title may have been confusing, and we changed it (see below). To summarize: The objectives of this study are 1) to quantify the discrepancies between observed and satellite imagery (MODIS) derived irradiance, and 2) to identify the key error sources of the discrepancies using broadband and spectral measurements. In the original manuscript, the general approach was introduced after the objectives (see **Line 5, Page 5**). As the reviewer states, the title may not have properly reflected the objectives, and we therefore changed it to "The effect of low-level thin Arctic

clouds on shortwave irradiance: Evaluation of estimates from space-borne passive imagery with aircraft observations".

It is always difficult to define the scope of a manuscript. In our case, we used the (limited) data from this study to assess to what extent satellite-derived estimates of irradiances under cloudy conditions (i.e., satellite-derived cloud radiative effects) are rooted in reality. To do so, we had to dive into the surface albedo as one of the parameters controlling the changes of irradiances by a cloud, as well as into the other drivers, finding in the end that the most important factor was (in our case) that MODIS simply didn't detect a significant fraction of these clouds. Indeed, we could have done many other things as well (for example, actually calculated net irradiances in the SW and LW to come up with the radiative effect of these clouds), but the emphasis was on the irradiances themselves, not on the derived quantity, the radiative effect. That said, we are not entirely sure what the reviewer meant by asking for the "full potential" of this paper. We would rather not re-write the paper to do something that was not intended in the beginning, nor do we feel that we should go beyond the scope of the paper because it is long as it is. Instead, we decided to clarify the objectives more, as well as emphasize the importance of the conclusions, which we do believe are strong.

We hope that changing the title, as well as clarifying the objectives (see details below) defines the scope better. We disagree that the conclusions are unclear; on the contrary, we actually think that the conclusions are rather succinct. At **Line 29, Page 13** in the original manuscript, the conclusions were clearly stated. Indeed, our study does raise many questions, particularly in the conclusions section. In our understanding, raising new questions based on observations is a justified and commonly accepted approach. We did answer the fundamental questions of this paper, which are (1) How well do satellite-derived shortwave irradiances compare with observations [caveat: we do so with whatever limited measurements we were able to use]; (2) what are the leading causes of any discovered discrepancies? As stated above, we found that the largest error source was the fact that MODIS does not detect the thinnest clouds. This finding begs the question whether this is true in regions of the Arctic other than our limited sample. We do think it is adequate to raise this question in the conclusion.

We did take to heart the reviewer's comment that the text might be easy to mis-interpret by the reader, and we carefully went through the individual comments below. We hope that changes in the manuscript make it more readable, and would like to again thank the reviewer for pointing out these issues.

Thank you also especially for the comments regarding the uncertainty. This was also raised by the other two reviewers, and constituted a significant omission. We spent considerable time and effort for an in-depth uncertainty analysis, especially in the estimates of the snow fraction from the aircraft imagery, on the SSFR-BBR irradiance product, and on the radiative transfer calculations based on MODIS retrievals. The details can be found in Appendix D (**Line 12, Page 17**), and the error bars can be found in many of the figures in the main body of the paper. After doing all of these, the message still stands, but we feel that it has become stronger.

2 Major comments

2.1 Unclear objective of the study

After reading the title and the introduction it is somehow unclear, what the manuscript aims to obtain: irradiance or the cloud radiative effects. The introduction does not match the title. The analysis and methods presented in the study also show not what was promised in the title: "Shortwave radiative effect" was calculated and discussed only briefly. Most of the analysis concentrates on irradiances. The introduction does not give an overview on how cloud shortwave radiative effects are commonly derived. In the analysis CRE is only discussed in two sentences. Neither the method and uncertainties are introduced nor are the values discussed. This does not justifies the title of the manuscript.

R: The manuscript aims to evaluate the irradiance derived from passive satellite imagery under cloudy conditions in the Arctic. A better understanding and error quantification of irradiances derived from satellite imagery is needed to better understand cloud radiative effects as well. The original title of the manuscript was chosen in that spirit. However, although cloud radiative effects are closely associated with the irradiance, our discussion on the CRE is indeed limited. We therefore agree that the title with CRE was misleading and we changed to "The effect of low-level thin Arctic clouds on shortwave irradiance: Evaluation of estimates from space-borne passive imagery with aircraft observations". After carefully thinking about changing the title as well as the fact that the CRE is not the main focus of this study, we decided to remove the two sentences that discussed the estimated CRE from the two cases, and focused the content solely on the irradiance evaluation.

"Imagery-derived irradiance": To me, this implies, that camera images are used and integrated into an irradiance. Or at least, that the irradiance is directly derived from images. That's not done in the manuscript and also not at all covered by the introduction. What the authors did is a parametrization of the surface albedo based on the sea ice fraction, which was observed from a camera. So I suggest to remove the word "imagery-derived" from the title.

R: What we meant by "imagery-derived irradiance" in the original title was irradiance derived from passive *satellite* imagery. In fact, the use of the satellite imagery (and derived products) is also explained in the paper: It is done by using the optical thickness and effective radius, derived from the radiances observed by MODIS, in radiative transfer calculations to calculate irradiance. These radiative transfer calculations also require the surface albedo, which is derived from a combination of the airborne radiometers (SSFR) and the *aircraft* imagery (camera). However, the aircraft nadir camera images were not used for any irradiance calculations. We only used the nadir camera images for estimating the snow fraction in the surface albedo parameterization. To clarify, we now used the word "space-borne passive imagery" in the title and elsewhere.

This misleading title leaves the reader searching for the actual objectives of the study. Unfortunately, also the motivation given in begin of the manuscript does not fit to what finally was achieved. E.g.:
"Validation of CERES-MODIS derived irradiance": In section 2, the authors state that one objective is to validate CERES-MODIS derived irradiance. This is confusing after reading the title and introduction. CERES irradiance is a different story compared to estimating the CRE. And I also do not see a CERES product in the study. The authors theirself state, that the design of the measurement strategy failed to compare to the CERES product. MODIS retrieval and own radiative transfer simulations are applied. However, on Page 13 line 36 the authors conclude, that CERES observations are used to constrain the observations. This was not done. To avoid confusion,

I suggest to remove CERES form the argumentation. Still, comparing irradiances is not the same as estimating the CRE.

R: "Validation of CERES-MODIS derived irradiance" was actually not the objectives of this study, nor was this stated in the manuscript. "Validation of CERES-MODIS derived irradiance" was mentioned when we introduced the ARISE field campaign. When talking about ARISE in general, we had to talk about its primary objective, the statistical validation of CERES/MODIS products, because this objective explains the "lawn mower" patterns, which were developed to cover multiple CERES footprints. However, this statistical comparison is a separate paper by other authors, which, however, has not been published yet. An AGU abstract can be found here:
https://ui.adsabs.harvard.edu/abs/2015AGUFM.C41D0753C/abstract
Whereas the CERES validation paper aggregates multiple CERES footprints in a 100 km x 100 km region and compares the aggregated products with the aircraft measurement PDFs in this same region, we here pursue a direct inter-comparison of MODIS-derived irradiances with aircraft observations on the pixel-level (pixel-by-pixel along the flight track). The distinction between the motivation of ARISE as a whole (the statement the reviewer picked up on), and our study is described in the objectives: 1) to quantify the discrepancies between observed and satellite imagery (MODIS) derived irradiance, and 2) to identify the key error sources of the discrepancies using broadband and spectral measurements. These were actually clearly stated at **Line 14, Page 4**.

Regarding this comment: "**The authors theirself state, that the design of the measurement strategy failed to compare to the CERES product.**", we are not sure where this is coming from; we did not say that the measurement strategy of ARISE failed to validate the CERES product. What we did say was that our paper follows a different approach, and that we did not intercompare CERES-derived irradiances with aircraft observations. Instead, we used MODIS-derived irradiances to compare with irradiance measurements at the pixel level. The basic idea is described in the BAMS paper of ARISE (Smith et al. 2017), and we anticipate that a paper about the direct comparison (see AGU abstract) will still be published.

We also did not state that the CERES observations are used to constrain the observations provided in *this* study. The original words from the manuscript were "While the calculations in the above-cloud case can be constrained through the TOA radiation product from satellite observations (CERES)". This was a *general* statement to emphasize that undetected clouds will be even more problematic for the surface energy budget than at TOA because CERES on Aqua and Terra constrains TOA fluxes more directly than those at the surface. To clarify, we rephrased to "While the radiation calculations at TOA can be constrained through the radiation product from satellite observations (e.g., CERES)". After adding clarifications in the text of the manuscript, we decided to keep the CERES related words in the revised manuscript to make the description of the ARISE campaign accurate and complete.

"longwave radiative effects": There is one section in the introduction on the longwave effect of water vapor on the surface radiation budget. But the title of the manuscript suggest, that the study is on solar effects only. So longwave radiative effects by water vapor is kind of irrelevant. The manuscript also does not include a study on the radiative effects of the water vapor profiles. Only the pure profiles are discussed.

R: It is true that the manuscript is focused on the shortwave radiative effects. We agree that the longwave effect of water vapor has no immediate relevance for this manuscript; we had initially included for context because insufficient knowledge of the water vapor may lead to uncertainties in the (surface) radiation budget rivaling those from insufficient knowledge about clouds. We decided to remove the discussion of the longwave effect of water vapor from the introduction of the revised manuscript.

We also acknowledge that the impact of insufficient knowledge about water vapor on the *shortwave* irradiance was not discussed thoroughly in the original manuscript. We used atmospheric profiles from MERRA-2 and aircraft data in the radiative transfer calculations, and they agreed well with the measurements in the water vapor absorption bands. In the revised manuscript, we checked the sensitivity with respect to water vapor by adding radiative transfer calculations with the climatological water vapor profile (in addition to the MERRA-2/aircraft-derived water vapor profile). The error contribution due to inaccurate water vapor knowledge is shown in Fig. 10 (see **Page 34**).

After all, I had the feeling that the manuscript shows a potpourri of separate analysis, without a clear major goal. This probably is not true, but the manuscript requires a more clear objective. From what I read, the study aims for a closure study, which validates the MODIS cloud product by airborne observations of irradiance. Could this be the major aim? Or do you aim identifying radiative processes in the Arctic atmosphere related to surface-cloud interaction?

R: As stated in the response to the general comments, we actually think our objectives were clear, but that they may not have been well enough formulated: 1) to quantify the discrepancies between observed and satellite imagery (MODIS) derived irradiance, and 2) to identify the key error sources of the discrepancies using broadband and spectral measurements. To do so, we first evaluate the key parameters that control the changes of irradiances by a cloud. Since the surface albedo, which is one of the before-mentioned key parameters, can be derived from the direct clear-sky measurements of SSFR, we developed a parameterization that utilized the surface context information from nadir camera imagery to account for the surface variability that the surface albedo parameterization can be used for cloudy calculations, which are the focus of this paper. After the surface parameterization, we discussed the model calculations with measurements from broadband and spectral perspectives and we discovered that the major error contribution is from MODIS not seeing the clouds. We added clarification about this on **Line 14, Page 4** in the revised manuscript.

I think it is important to clarify the main objective of the manuscript and concentrate on the major aspects needed to achieve these goals. If the aim is a closure study, then I suggest to remove the estimation of cloud radiative effects, which currently is misleading. Or at least shift the calculation of CRE to the end of the study, after the irradiances have been compared. This would allow to extend the validation for CRE based on the uncertainties/conclusions which have been found already before when comparing the irradiances.

R: Thanks for your suggestions on several different ways of clarifying and concentrating on the main objectives of the paper. We realized that the CRE aspect of this paper was confusing, and we decided to remove the estimated CRE from the manuscript as well as the title. We also modified the text at the beginning of the Data and Methods section (see **Line 14, Page 4**) to make the objectives more clear. We hope the message will become clear in the revised manuscript.

2.2 Methodology needs to be outlined

Several comparisons of different quantities (albedo, irradiance above, below clouds) are shown in the manuscript. However, it is not always clear what the purpose of each individual step is. The general and also the specific methodology of the analysis should be outlined. In the conclusion the authors write about "developing a validation approach". I don't see a clear validation approach in

the study. If there is a strategy, then this needs to be outlined precisely in the begin of the manuscript. Maybe any schematic showing the different comparisons broadband, spectral, flight one, flight two might help.

R: Thank you for your comments. The primary goal of this study is to evaluate the radiative transfer calculations of irradiance derived from cloud optical properties provided by passive remote sensing in the Arctic, identify the error sources in the radiative transfer calculations and quantify the error contributions. To do so, we had to try our best to make the surface albedo right using the aircraft measurements. That's why we first provided the surface albedo parameterization. After we obtained the most "suitable" surface albedo set, we evaluated the irradiance under cloudy conditions for above-cloud case and below-cloud case. We intended to use above-cloud case as a proxy to evaluate how well satellite-derived irradiances represent the reality, and below-cloud case as to assess the realism of satellite-derived surface budget parameters (specifically, the downwelling and upwelling irradiance). As one can see, the elements of the paper together are prerequisites to understanding the realism of satellite-derive CRE as well, although we are no longer talking about CRE in the paper (as suggested by the reviewer) to avoid confusion. To make it more clear, we added more detailed description about the steps at **Line 5, Page 5**. The "developing a validation approach" was more of an outlook. The study was not about developing a validation approach, it is a hypothesis study. Thanks for your suggestions on outlining the strategy.

It is also confusing, how and when the data of both flights is used. It took long until I understood, that the two flights provide different observations (high vs. low flight altitude). I suggest, that the authors clearly report, what is different between both flights. Why two cases are needed and how the observations are mixed/combined in the study?

R: In the original manuscript, we had the flight information at **Line 2, Page 10**. As stated, for 2014-09-11 (also referred to as above-cloud case), the aircraft measurements were taken when aircraft flew high around 6.5km. However, for 2014-09-13 (referred to as below-cloud case), the aircraft measurements were taken when aircraft flew low at around 200m. The ARISE campaign was designed that flights were either above or below a cloud field, but almost never both (because of sampling time limitations). For this reason, we needed to study two distinct flights to evaluate at above-cloud and below-cloud budget parameters (irradiances). We did not mix or combine the observations of the above-cloud case and below-cloud case together because they occurred on different days.

Similarly, the motivation of section 3.1 was missing and leaves many open questions when reading the section. These questions should be addressed before starting the analysis:
What is the purpose of this analysis and of the parametrization of surface albedo with snow fraction? I only can guess. Wasn't surface albedo measured directly with BBR and SSFR? Where is the need to parameterize surface albedo if albedo is measured anyway?

R: The BBR/SSFR can directly measure the surface albedo, but not under all conditions, specifically, when clouds were present. Only clear-sky conditions could be used to calculate the surface albedo. These are a rare occurrence because the low-level clouds were ubiquitous. The main driver for the variability of the surface albedo was the snow fraction, and therefore we decided to couple the (rare) direct albedo measurements to the camera-derived snow fraction, which is more readily available, even under partially cloudy conditions. In addition, we could then use the snow fraction as a single "tuning" parameter, which ensured that the calculated upwelling irradiance measurements were in agreement with the measurement above cloud. In short, that is why we used the data aggregation technique, which used a small collection of low-level clear-sky aircraft measurements to parameterize the surface albedo. After the

parameterization, one can retrieve surface albedo for 1) the above-cloud case study, where the clouds cover the surface and the surface albedo cannot be directly measured, 2) the below-cloud case study, where the clouds block the sun and the surface albedo cannot be directly measured. Moreover, the albedo parameterization was our simple way to account for the surface variability in the Arctic using a collection of data. We clarified this in the revised manuscript (see **Line 35, Page 10**).

As the surface albedo properly is an input to the radiative transfer model, section 3.1 should be presented before explaining the radiative transfer simulations.

R: Thank you for your suggestion. However, we preferred to put the surface albedo in the Results section because the spectral surface albedo was crucial for the radiative transfer calculations and can be considered a stand-alone crucial result of the study along with the irradiance validation.

2.3 Only limited conclusions

The conclusion section does contain a lot of "may"s and "if"s. More questions are raised than answered. The authors theirself are hesitant to draw conclusion: "sheds some light on these questions", "the actual surface albedo may deviate from commonly used climatologies", which is more than obvious. Also the limitations of the limited data set for conclusions is acknowledged. Based on these little new results, the entire section, especially the last part of the conclusion read more like an outlook, indicating, that the study did not improve much. It is not mandatory to make big improvements, but I also do not see any method, approach on how to improve all the issues that are summarized in the conclusion section. To improve the manuscript it would be helpful to present and discuss a method or approach of how to perform validation studies based on similar measurements as shown in the study. As mentioned by the authors, there is potential to process more data from the airborne campaign. To do so, a clear approach with step A, B, C,... should be presented in the manuscript.

R: Thank you for your comments on the conclusion. We changed the wordings where contains “may”s and “if”s to avoid the misinterpretation of a weak conclusion. We wanted to point out that we do not aim to provide a validation approach that can be applied widely to other observations. Instead, this paper is more about a hypothesis study. We are not aware that we were hesitant drawing conclusions. Yes, it is indeed more than obvious that the real surface albedo deviates from the true albedo. At the same time, there is currently no operational product of the spatially and temporally varying surface BRDF (albedo), unlike in most other regions of the world, where this product does exist. Since this is such a big problem, we do believe that even such an obvious statement is warranted. However, this was not the most important part of the conclusions, which was focused on clouds:

We discovered the MODIS misses about 27% of the low-level thin clouds in the Arctic. This had been suspected by earlier studies, but is now confirmed with our data. We do not agree with the reviewer that this is a “weak” conclusion. If this under-detection is a common occurrence throughout the Arctic, the surface budget and melt assessments based on satellite observations could be quite different.

In addition, we presented some lessons learned from ARISE. Most importantly, the separate sampling of above- and below-cloud irradiance in separate flights was not ideal because it impedes a true radiative closure study. This is an important message to be considered in future Arctic field campaigns.

2.4 Uncertainty Analysis

The study aims comparing measured irradiance with simulations. As the data is intended for use in a comparison study, a discussion of the measurement uncertainties is fundamental. No uncertainty ranges are indicated in the plots.

R: Thank you very much for your comments on the uncertainty analysis. As we realized the uncertainty analysis is very important and was missing in the manuscript, so we added it in Appendix D (**Line 12, Page 17**) of revised manuscript. More importantly, we also added the estimated uncertainties of the measurements and calculations in the plots.

BBR: What about the accuracy of the data? What is considered in the data processing? Are the BBR instruments actively levelled? The SSFR is levelled. What makes this for a difference comparing SSFR and BBR?

R: The accuracy of the BBR data is 3%. In contrast to SSFR, the BBR instrument was fix-mounted to the skin of the aircraft. We added this information in the revised manuscript (see **Line 16, Page 5**). A software attitude correction (Long et al., 2010 was applied to BBR data to account for the change of solar position due to aircraft pitching and rolling. Neither the BBR zenith nor the nadir light collector were actively aligned. Only the SSFR zenith light collector was actively aligned. After applying attitude correction for both SSFR and BBR, they shouldn't be much different from a radiation measurements perspective while the aircraft was flying fairly smooth at a slightly positive but stable pitch angle. Without the active leveling, the radiation measured by BBR can be contaminated from side when the aircraft pitched or rolled at a large angle. Since the data was filtered out when the aircraft was ascending, descending or turning, BBR and SSFR should be consistent (the degree to which they are is discussed in the Appendix D, see **Line 12, Page 17**).

The same holds for SSFR. What are the final uncertainties? How the radiometric calibration contributes to the uncertainties? What is more important, correcting the angular response or tracking changes of the radiometric sensitivity over time?

R: This is now described in the revised manuscript (see **Line 12, Page 17**). SSFR and BBR are merged into a combined irradiance product, which relies on the higher absolute accuracy of the broadband measurements from BBR and the spectral resolution of SSFR.

P10 L13: There are several sources of uncertainty in the determination of the surface albedo. How the estimation of the surface albedo affects the uncertainty of the final results/study? Also extend the discussion of uncertainties by the MODIS cloud retrieval. Only undetected clouds have been considered so far. What about cloud phase, the second thin cloud layer, surface albedo assumed in the retrieval?

R: We added an uncertainty analysis for the surface albedo as well as a discussion of how it propagates into irradiance calculations to the revised manuscript (see **Line 12, Page 17**). After we obtained the uncertainties for the SSFR-BBR combined irradiance product (see **Line 12, Page 17**), the uncertainty of the surface albedo was done through error propagation. The details can be found in the revised manuscript (see **Line 12, Page 17**). We updated the figures contains the surface albedo results with error bars.

In addition to the uncertainty estimate for the surface albedo, we also included the uncertainty of the MODIS cloud retrieval. Based on the cloud phase from MODIS cloud products, only 2% of the clouds were identified as ice clouds. In addition, limited in-situ measurements showed the majority of the clouds were liquid. Therefore we considered only liquid clouds in this study. Since we were not aim to provide a closure study but hypothesizing MODIS cannot detect a portion of thin clouds, the second thin cloud layer (cirrus) was not considered in this study. We have added a comment to this effect in the manuscript (see **Line 14, Page 11**). The surface albedo assumed in the cloud retrieval was included in Figure 5 for comparison.

3 List of specific comments

P2 L9: From the abstract it is not clear, why two independent estimates of the surface albedo (from SSFR/BBR and from the camera imagery) are needed?

R: These estimates are not independent. The camera and BBR/SSFR are used jointly as explained in the paper and also above in this response.

P2 L16: How large is the radiative effect of the non-detected clouds? This is an important value when MODIS misses a significant faction of clouds.

R: The shortwave cloud radiative effect (CRE) of the non-detected clouds is about -40 Wm^{-2}. Since we changed the title of the manuscript by removing the shortwave radiative effects, we decided not to include the discussions for shortwave CRE in the manuscript.

P3 L14: The study by Hartmann and Ceppi (2014) does not fit to the topic of cloud radiative effects. Direct radiative effects by sea ice loss has nothing to do with clouds unless you argue, that the expected increased cloud cover over increased area of open water is not able to compensate the reduced reflection of solar radiation by the surface.

R: We agree that Hartmann and Ceppi's paper does not fit the topic of cloud radiative effects but we decided to keep their paper here for two reasons. First, Hartmann and Ceppi's paper shows the application of satellite remote sensing in the Arctic to study sea ice extent. Since the radiative effects caused by sea ice loss are associated with albedo feedback, the surface albedo is relevant to what we discuss in our paper. Secondly, Hartmann and Ceppi's paper can be used as a good introductory to bring up the following study by Kay and L'Ecuyer (2013), which discussed the cloud radiative effect and associated sea ice loss in the Arctic.

P3 L17: Explain acronyms CERES-EBAF, 2BFLXHR-LIDAR.

R: The full name of CERES-EBAF is Clouds and Earth's Radiant Energy Systems – Energy Balanced And Filled. The 2B-FLXHR-LIDAR represents level 2B radiative fluxes and heating rates calculated from radiative transfer model by utilizing radar-lidar cloud and aerosol. We made changes to the revised manuscript (see **Line 18, Page 3**) to introduce these acronyms.

P4 L2: This presented state of the art on spectral albedo of Arctic surface types is very pessimistic and does not consider recent publications which cover a lot more data also derived from airborne observations (areal and temporal variability):

Perovich, D. K., Tucker, W. B., and Ligett, K. A.: Aerial observations of the evolution of ice surface conditions during summer, J. Geophys. Res., 107, SHE24-1–SHE24-14, https://doi.org/10.1029/2000JC000449, 2002.

Malinka, A., Zege, E., Heygster, G., and Istomina, L.: Reflective properties of white sea ice and snow, The Cryosphere, 10, 2541–2557, https://doi.org/10.5194/tc-10-2541- 2016, 2016.

Malinka, A., Zege, E., Istomina, L., Heygster, G., Spreen, G., Perovich, D., and Po- lashenski, C.: Reflective properties of melt ponds on sea ice, The Cryosphere, 12, 1921–1937, https://doi.org/10.5194/tc-12-1921-2018, 2018.

R: Thank you for the providing these references, which we added. However, our pessimistic view on spectral surface albedo of Arctic inhomogeneous surface originally came from a space perspective (see earlier comment on the lack of an operational product). We weren't being very inclusive about the most up-to-date spectral surface albedo studies for different surface types in the Arctic. We did add more discussion at **Line 2, Page 4** for the provided references.

P4 L29: Fairbanks is in the center of Alaska. Where did you fly over Arctic sea ice? Figure 1: Add longitude and latitude.

R: These two cases were within the following region: longitude west of -136°, longitude east of 130°, latitude south of 72°, latitude north of 74.5°. Thanks for the suggestion. We added the longitude and latitude to Figure 1.

P6 L22: Were cloud properties derived from the SSFR measurements? If not, I suggest to remove this statement here.

R: No, the cloud properties were not derived from SSFR in this paper. That said, retrieving cloud optical properties from SSFR measurements is a common application of SSFR. Despite that, we removed this sentence from the original text to avoid confusion.

P6 L26: What is the resolution (number of pixel) of the camera? What type of lens is used (distortion-free?)?

R: The resolution of the image extracted from nadir video camera is 2592*1952. It is a standard, commercially available video camera. We added this information in the revised manuscript (see **Line 2, Page 7**).

P7 L4: Instead of using such an interpolation technique, could you determine the vignetting effect by measuring over a white almost Lambertian surface? I could imagine, that a snow covered surface could provide this as a first approximation. For your application this should be sufficient. Or use a certified diffuse reflector.

R: Thanks for your suggestion. It is a good idea to determine the vignetting effect my measuring over a white surface. However, by manually going through the nadir camera images, we could not find an all-white image. Fortunately, our sensitivity study showed that the error contribution in snow fraction from the interpolation factor was minor comparing to other factors (see Appendix D). This is because the corner points of the image (most affected by the vignetting effect) are removed from the snow fraction estimation.

P7 L5: "Black" means probably "dark" like the dark signal of a non-illuminated camera sensor? In terms of radiation I would prefer "dark". Black is a color and limited to visible wavelength.

R: Actually the "black" matrix here means the matrix contains value of 0 (color black). This is an extrapolation technique explained in Haeberli and Voorhies 1994 (see explanation in the manuscript). We applied the described image processing technique to the nadir camera imagery data to estimate the snow fraction. However, the nadir camera imagery did not provide any radiation data (radiance or irradiance).

P7 L5: How the 2D matrix was determined? Each camera and lens system must have an individual matrix.

R: The 2D matrix was manually set to compensate for the vignetting effect. The nadir camera was the only camera we used to estimate the snow fraction.

P7 L15: Can you discuss the retrieved snow fraction of the example and the uncertainties/quality of the method in this section? Only referring to the figure is not sufficient.

R: Thank you for your comments. We added the uncertainty discussion of snow fraction estimated from nadir camera image using adaptive thresholding method the in Appendix D.

P7 L16, Figure 2: Figure 2a shows the presence of thin gray ice, which is not detected as sea ice in Figure 2b. This means, that from a physical view, the sea ice fraction is underestimated. Although, optically these areas are less bright, they have a higher reflectivity and might bias your results.

Can you give an uncertainty estimate, how the sea ice fraction will change with adjusting the threshold between bright and dark pixel?

R: Thank you for the comments on Figure 2. We acknowledge the limitations of the adaptive thresholding method and the uncalibrated nadir camera imagery. However, we do believe that we were able to quantify the snow fraction sufficiently well to subsequently parameterize the surface albedo. To address the reviewer's concern, we conducted a sensitivity analysis (added in the Appendix D).

As the camera provides RGB images, it should also be possible to classify different ice types following the methods describes by Perovich et al., 2002. Did you thought about this?

Perovich, D. K., Tucker, W. B., and Ligett, K. A.: Aerial observations of the evolution of ice surface conditions during summer, J. Geophys. Res., 107, SHE24-1–SHE24-14, https://doi.org/10.1029/2000JC000449, 2002.

R: No, we didn't thought about the method by Perovich et al. 2002 for the original manuscript. Perovich et al. used a histogram thresholding method, which manually set threshold for the histograms of image RGB values to identify different surface types. We began our snow fraction estimation from the histogram thresholding method by using threshold value from the bimodal distribution of the image grayness. However, the method became problematic during automation because the bimodal feature was not clear for all the images and the estimated snow fraction was not accurate by the judgment of human eye. That's why we turned to the adaptive thresholding method. Due to the fact that the nadir camera is not radiometrically calibrated and our major goal was to get only an estimate of snow fraction from the image, we kept the albedo work fairly simple but good enough for automation. The Perovich method is very valuable if done with appropriate equipment. We didn't have that equipment, and the purpose of our study was a different one. In future campaigns monitoring the evolution of sea ice albedo, the Perovich method should be used. We think Perovich et al.'s paper is a great reference so we added a brief description at **Line 4, Page 4** in the revised manuscript.

P7 L30: For altitudes above 6.5 km, a standard atmospheric profile is used. Aren't there any radio soundings available? Barrow? What about dropsonde releases from the aircraft?

R: We did not use the standard atmospheric profile directly. Instead, we used either the atmospheric profile from a) aircraft itself or the atmospheric profile from b) MERRA2 reanalysis data at the closest

location of the average location of the flight for the atmospheric profile below 6.5 km. For the atmospheric profile above 6.5 km, we first rescaled the standard atmospheric profile with the end point of a) or b) and stitched them together to provide atmospheric profile from the surface to the top of the atmosphere. The radio soundings are available at Barrow but it's far away from the area where the aircraft flew, so the reanalysis was preferable. We did not have any dropsondes on the aircraft. For future campaigns, this will be a must-have.

P8 L3: It would be helpful to include a figure showing a time series or similar plots of the MODIS COPs which are extracted along the flight path. Just to know, what range of COPs have been present and how variable the cloud field was. What about temporal offsets between MODIS and airborne observations?

R: The MODIS COPs time series and time offset between MODIS and airborne observations are shown in Figure 7. The COPs range from 0 to 16 during the above-clouds case flight (2014-09-11). The temporal offsets between MODIS and the airborne observations range from 0 minute to 50 minutes (flight from 21:10 to 22:45 and the MODIS granule was at 22:00).

P8 L4: All clouds are assumed to be liquid. Is there any prove for this? In situ observations? The temperature profiles are well below 0°C where mixed-phase clouds typically are often present.

R: The MODIS cloud phase product shows less than 2% of ice clouds present along the flight track. Of course, the phase detection under these conditions is not reliable. Limited in-situ observations were available (forward scattering probe; imaging probes), and they suggested that the clouds primarily consisted of liquid water. We added a brief statement in the revised manuscript to that effect (see **Line 23, Page 8**).

P8 L11: What quantities are included in the atmosphere profile? I usually understand also temperature and humidity to be part of the atmospheric profile, but there are provided separately.

R: The atmosphere profile includes the temperature and humidity as well as other atmospheric constituents, such as methane, carbon dioxide, ozone etc. We changed the bullet points structure where temperature and humidity were contained in the atmosphere profile (**Line 32, Page 8**).

P8 L16: What albedo is assumed here?

R: By using method For the 2014-09-11 (above-cloud case), the surface albedo used parameterized albedo with snow fraction of 0.764. In the revised manuscript, we explain how we arrived at that value (see **Line 38, Page 10**). For the 2014-09-13, the surface albedo at each point along the flight track is calculated based on the snow fraction estimated from the nadir camera imagery.

P8 L17: Specify or provide the slit function in the instrument description.

R: We added the slit function information– "… full width at half maximum (FWHM) of 6 nm for silicon channels and FWHM of 12 nm for InGaAs channels" (see **Line 2, Page 9**).

P8 L19: Does MODIS provide cloud base?

R: No, MODIS does not provide cloud base.

Section 2.5: The description of the radiative transfer simulations should be separated from this MODIS section. The title of the section does not suggest that it will include the methodology of how the solar irradiance is derived. I suggest to add a separate section "methodology". See general comments.

R: Thank you for your suggestion. We introduced the method after the introduction of each instrument in the section of Data and Methods. It will not be necessary to add a separate section "methodology". Instead, we added the description of steps at the beginning of the "Data and Methods" to outline the general approach (**Line 5, Page 5**). In addition, we changed the section to "Radiative Transfer Calculations based on MODIS Cloud Products".

P10 L8: Why the albedo for 11 September needs to be calculated/constructed? I'm lost ... If you have the ice fraction, why there is now surface albedo measurements?

R: On 11 September, the aircraft took measurements high above the clouds, where the surface albedo cannot be directly obtained from measurements. Instead, we used the data from 13 September, which led to the parameterization of surface albedo via snow fraction as described earlier. We used that parameterization (with a snow fraction of 0.764, see above) for 11 September since the aircraft was flew in a similar area as on 13 September.

P10 L9: I was wondering, why you use "snow fraction" instead of the more common "sea ice fraction" or "cover". Likely because there is dark snow-free sea ice. Can you elaborate the term "snow fraction" more clearly in section. 2.3. This would help the readers to understand immediately, that there is a difference to sea ice fraction and why this is relevant.

R: The definition of this fraction is as follows: number of bright pixels divided by the total number of pixels in the nadir camera image. Since we don't know whether the bright pixels were snow or ice or both, we assume the bright pixels are snow most of the time. Thus we named it "snow fraction". The dark pixels, on the other hand, might be either open ocean or "young" sea ice. The latter is supported by its spectral shape (see **Line 23, Page10**).

P10 L17: How the cirrus is considered in the analysis? How strong does it influence the final results? Especially with respect to the proposed CRE of clouds?

R: We did not include any cirrus in the radiative transfer calculations (see response for "**P11 L18** …"). From Figure 7, the cirrus affected the downwelling irradiance by about 30 Wm^{-2} at most.

P10 L23. Figure 7b: There is a large mismatch for areas where no clouds are detected. How strong, the undetected clouds can change the irradiance? I guess, the difference in the "cloud-free" areas is more due to the surface albedo (sea ice fraction) than due to the clouds. $\tau = 0.5$ would not make much difference over bright snow surface. In optically thick areas, the agreement is better. How strong e.g. 10% uncertainty of the sea ice fraction would influence the results here? Can you rule out any change of the sea ice fraction along the flight track?

R: We cannot rule out a change of the snow fraction along the flight track. In fact, this is rather likely. Relevant for our study is that the calculated irradiances jump abruptly near the edges of the clouds as retrieved by MODIS, whereas the measured irradiances vary smoothly, suggesting that the clouds continue beyond the "sharp" edges as detected by MODIS. This is simply due to the optical thickness

detection threshold of MODIS. Our findings are further supported by photos from the camera. Changing the snow fraction by a certain number would change the upwelling irradiance, but it would not remove the jumps in the calculations and bring it into closer agreement with the measurements. In optically thick areas, the measurement-model agreement is better, simply because the surface has less of an impact on the upwelling irradiance.

P10 L33-37: These general details of the cloud conditions that have been present during the two flights is needed much earlier. I also suggest to add a comparison of the differences between both observed cloud cases. Otherwise, it is hard to follow the analysis.

R: Thank you for your comments. We changed the name of the cases to "0911-above-cloud" and "0913-below-cloud" to avoid confusion at **Line 30, Page 10**. Since the cloud optical thickness (cloud conditions) was provided for "0911-above-cloud" and "0913-below-cloud" in Figure 7 and Figure 8, we decided to introduce the cloud condition for each case when the figures was discussed. The details for "0911-above-cloud" flight is at **Line 12, Page 11** and the details for "0913-below-cloud" flight is at **Line 2, Page 12**.

P10 L40: So far it was not clear, that for the first case, the albedo was fixed. This needs to be made clear at the begin of the analysis. What are the differences between both cases?

R: We added clarifications in the revised manuscript (**Line 35, Page 10**). Although using the same parameterization, the spectral surface albedo was fixed for the above-cloud case. For the below-cloud case, the surface albedo was calculated based on the snow fraction estimated from the nadir camera image.

P11 L2: I don't understand, why also for this case the parametrization is used. Isn't the parametrization based on the same data? What are the advantages of this approach?

R: The parametrization did not use the same data. The parametrization used the data collected under clear-sky condition on 2014-09-13. For the irradiance evaluation of the below-cloud case, due to the presence of clouds, the surface albedo cannot be directly measured, but it can be derive via the parameterization as long as the snow fraction can be retrieved from the camera imagery.

P11 L14: As I understood, the two days are different in a way, that once the aircraft flew above the cloud layer and once below. This means, that the CRE is defined differently for both cases. So how this is accounted here?

R: Yes, the two days are different. Due to the different cloud fields from two days, the study is limited to draw conclusions about the CRE for different cases (once the below-cloud, and once the above-cloud CRE). It is worth mentioning that this limitation of ARISE was one of the motivations to propose a new field campaigns with flight plans of flying both above and below for the same cloud field. Yes, the CRE was defined differently for both cases. Therefore, we did not draw any conclusions by saying it is a closure study of CRE.

Section 3.2. What is the benefit of having both BBR and SSFR broadband irradiance here? Why SSFR was integrated to broadband values and compared to BBR? This makes only sense, if e.g. surface albedo is once considered spectrally and once with a fixed broadband value? Or is there any other purpose?

R: The SSFR and BBR were used to validate the radiative transfer calculations. BBR was more accurate, but SSFR had spectral resolution, as described above. SSFR's azimuthal response was not isotropic

(unlike BBR's), and it was corrected with BBR's response during a dedicated calibration flight. After azimuthal correction, the SSFR downwelling irradiance was scaled to BBR using the method described in Appendix D. It is in this sense that SSFR and BBR data were "merged". However, they are not identical. Instead, a correction factor is applied to SSFR data that depends on the sun-sensor geometry. Since the calibration flight and the science flight occurred at different sun-sensor geometries, the broadband irradiance derived from SSFR and measured by BBR may deviate slightly from each other. We show them both to check for consistency between both methods. We need to show SSFR (in addition to just BBR) because we later use spectral irradiances from SSFR only to draw conclusions.

P11 L18: Where the "model-measurement biases in the broadband shortwave CRE" are discussed? The different values in Table 1 and 2 have not been explained. How the different CRE are calculated? How CRE is derived based on measurements and how it is derived based on the simulations? If there are estimates based only measurement, you would need cloud free flight sections, which I do not see in the data. How the cirrus layer is considered in the estimation of the CRE and the radiative transfer simulations? You cannot neglect the cirrus.

R: We no longer show the CRE calculations to avoid confusion (see above). Even Cirrus was indeed present during some of the flight segments, we did indeed not include it in the calculations. That is because MODIS does not distinguish between Cirrus and low-level clouds. MODIS derives the column-integral of optical thickness regardless of its vertical location. Of course, the measured downwelling irradiance is lowered under Cirrus clouds, and as a result the upwelling irradiances will also be lower than under Cirrus-free conditions. However, what mattered for the manuscript were the low-level clouds. We added a statement to this effect in the manuscript (see **Line 14, Page 11**). Of course, we would have needed to account for Cirrus if the purpose of the manuscript were a closure study.

P11 L21: Upward or downward irradiance?

R: It's the upwelling irradiance. We changed the text to clarify (**Line 32, Page 12**).

P11 L25: I don't understand, why you need a climatological surface albedo, when you measured and parameterized the albedo.

R: The climatological surface albedo was used to put our study in context with others, and to illustrate how much different surface albedos can affect the radiative transfer calculations.

P11 L28: Was the surface albedo fixed or varied in the simulations or do I misunderstood this sentence? That a fixed albedo will not represent reality is more than obvious. That's why I don't fully understand the approach to use a fixed albedo here. How is this motivated?

R: The surface albedo was fixed for the 11 September case (referred to as "0911-above-cloud") but varied for the 13 September case (referred to as "0913-below-cloud"). As we discussed in previous response, the surface condition was unknown when the aircraft was flying over clouds. When the aircraft was flying below clouds, we could not directly obtain surface albedo from measurements because the downwelling irradiance was varying with clouds. Using a fixed surface albedo derived from clear-sky measurements was the best we can do for the above cloud case. We tweaked the surface albedo until the clear-sky radiative transfer calculations matched with measurements at 1640 nm. We added this discussion in the revised manuscript for clarification (**Line 35, Page 10**).

P11 L29: Specify. Range of what?

R: The range here means the irradiance range from previous sentence. After revision, this text was removed.

P11 L31: Climate models? How you can draw this conclusion? No climate model is applied, analyzed or discussed in the manuscript. Even when a climate model would have been considered, the "underestimation" may only hold for your specific case, where the albedo is assumed to be too high. This must not hold for the climate models. Further, there are climate models available, which use sophisticated snow albedo parametrization accounting for different sea ice types, melt ponds, snow etc. E.g.:

Dorn, W., Rinke, A., Köberle, C., Dethloff, K., and Gerdes, R.: HIRHAM–NAOSIM 2.0: The upgraded version of the coupled regional atmosphere-ocean-sea ice model for Arctic climate studies, Geosci. Model Dev. Discuss., https://doi.org/10.5194/gmd- 2018-278, 2018.

R: We meant that based on the specific case study provided in the paper, the irradiance calculated from the climate models that used the biased surface albedo would be underestimated. We removed the text to avoid confusion.

Also, thank you for the reference. Although Dorn et al. (2018) used a sophisticated snow albedo parameterization accounting for different surface types, the surface albedo they used is a broadband surface albedo, no spectral surface albedo was used. In our paper, we strive to deliver two messages about the surface albedo 1) the spectral surface albedo is important, 2) accounting for the surface variability is important.

P12 L17: Please write the equation using the symbols of the quantities which are calculated here, not x, y.

R: We revised the equation by changing the symbols. In the manuscript, the equation was changed to $r = a - e^{b \cdot COT + c}$ at **Line 36, Page 13**.

P12 L19: The behavior shown in Fig. 11 can be explained by the change of surface albedo between cloud-free (direct Sun illumination) and cloudy conditions (diffuse illumination). A Similar behavior is reported by Gardner and Sharp (2010). This means, that you albedo is not necessarily wrong. It depends on what you want. A closure study comparing the irradiance in cloudy conditions required the cloudy-sky albedo. For estimating the CRE, the cloud-free albedo needs to be applied in the radiative transfer simulations.

Gardner, A. S., and Sharp, M. J. (2010), A review of snow and ice albedo and the development of a new physically based broadband albedo parameterization, J. Geophys. Res., 115, F01009, doi:10.1029/2009JF001444.

R: This is a good point. The basis of our paper is essentially the “blue-sky” surface albedo because that is what we were able to measure. The “white-sky” surface albedo (i.e., the surface albedo under cloudy conditions) does indeed differ from the blue-sky albedo, but we could not measure it for this campaign. For future campaigns, we hope that this can be done. What we see in Figure 11 (transition from 0 to non-

zero optical depth) could indeed be caused by this difference. We have added a comment to this effect in the manuscript (see **Line 5, Page 14**).

P12 L20: Figure 11 and the parametrization is shown for broadband quantities. Figure 12 is calculated spectrally resolved but used the broadband parametrization? Shouldn't the parametrization be computed for each wavelength?

R: The Figure 11 shows the entire fitted function - upwelling broadband irradiance ratio as a function of cloud optical thickness. In Figure 12, the parameterization was computed separately for each wavelength first. Then two ratio values are obtained for each wavelength parameterization: one at cloud optical thickness equals to 0, indicating clear-sky; and one at cloud optical thickness of infinity, indicating cloudy.

P12 L20: "Spectrum" of what? Upward downward irradiance or albedo?

R: The spectrum here means the upwelling irradiance ratio, which is the ratio between radiative transfer calculations of upwelling irradiance and SSFR measured upwelling irradiance. We changed the "spectrum" to "spectrum of ratio" at **Line 39, Page 13** in the revised manuscript to make it more clear.

P12 L20: **What is x? COT? If yes, then write COT. Also a bracket is missing in line 21.**

R: Yes, the x is COT. We changed the x to COT in the text and added the missing bracket.

P12 L23: "remarkable agreement". Without uncertainty estimation you cannot judge about an agreement.

R: Thanks for your comments. We added the uncertainty analysis in the Appendix D and the results still indicate good agreement between radiative transfer calculations and observations within uncertainty. We removed the sentence of "With these qualifications in mind, the agreement between MODIS-derived and measured irradiance is remarkable" to avoid making subjective statements.

P12 L33: If the major aim of the study is to show how good irradiances or the CRE can be derived from the MODIS cloud product, the most general scenario should be considered as well. The general case is, that you do not have any airborne observations. Which means, you have to rely on the surface albedo product of MODIS. Atmosphere profiles from reanalysis, etc.. This would be the routine/operational approach. Based on that, you may try to improve the approach by exchanging different assumption with the airborne observations, such as measured surface albedo.

R: We agree. When aircraft observations are not available, the dominating error by far as far as the estimated shortwave fluxes go would be that of the fixed (assumed) surface albedo, which makes an operational surface albedo product so important. However, the point of the manuscript was not just about the flux validation. We hypothesize that MODIS might generally under-detect clouds (regardless of the shortwave fluxes, and regardless of the surface albedo).

P2 L38: You did not discuss deeply the uncertainties of the MODIS retrieval. The comparison only shows, that there are differences, but could you use the observations to constrain which COPs have been retrieved wrong and to what degree?

R: Thank you for your comments. We added the uncertainty analysis for the radiative transfer calculations, which included the uncertainty of MODIS cloud retrievals (in Appendix D, **Line 12, Page 17**).

P13 L1: The impact of water vapor profiles was not shown in the manuscript.

R: We added the few calculations with different climatology atmospheric profiles and the results are added in Figure 10. We also added the discussions at **Line 21, Page 13**.

P13 L3: "developing a validation approach": I don't see a clear validation approach in the study. If there is a strategy, then this needs to be outlined precisely in the begin of the manuscript and summarized here.

R: Thank you. The validation approach was not clearly described. We added the description of the validation/evaluation steps at the beginning of the manuscript (see **Line 5, Page 5**) to avoid confusion.

P13 L15: It seems, that the study presented here could not answer any of the questions written in this section. I suggest to start the conclusion section with conclusions and not rise more questions than have been pointed out in the introduction.

R: Thank you for your suggestion. We did raise more questions here, but we think that is adequate (see also our response to the general comments). Our questions are meant as impetus to improve the observing system in the Arctic, or at the very least design future aircraft missions differently such that the questions can be answered. Such missions could (among other things) be motivated by the hypothesis developed here in this paper.

P13 L35: Define "excellent"! Why you consider the agreement excellent? Any objective measure to judge this? Excellent compared to what? This requires an uncertainty estimation.

R: The description as "excellent" agreement was for the comparison between irradiance calculations with SSFR-BBR irradiance when clouds were detected by MODIS. Of course, any of these qualifiers are relative, and all that can be said is that calculations and observations agree within their uncertainties. We added the uncertainty for both the calculations and measurements and changed the "excellent agreement" to "… agreed … within the range of uncertainties" at **Line 19, Page 15**. We do think that the agreement between calculations and observations is remarkable, provided that MODIS detects the clouds. That is an encouraging result for the quality of the cloud retrievals.

Appendix A: Can you briefly explain the concept behind these calculations? Is this done to derive the diffuse fraction based on the present cloud cover? What about broken clouds? Is this covered by the approach?

R: The concept is to perform diffuse/direct correction spectrally on SSFR measurements based on the broadband measurements from SPN-1 and spectral calculations from radiative transfer model under clear-sky. This approach covers clear-sky ($f = 1$), broken clouds ($0<f<1$), and cloudy ($f = 0$).

P15 Eq 1: Avoid the large slash.

R: We replaced the large slash with horizontal line. Now the equation is

$$f = \frac{(1 - DR_{SPN1}) \cdot \int_{\lambda_1}^{\lambda_2} F_{clear}^{\downarrow}(\lambda) d\lambda}{\int_{\lambda_1}^{\lambda_2} F_{clear}^{\downarrow}(\lambda) \cdot \left(1 - DR_{clear}(\lambda)\right) d\lambda}$$

P15 Eq 2: This equation was already given above.

R: Thanks for noticing the duplicate equations. We removed the repeated one.

P15 L24: How the boundaries of the image are treated if the subdomain is that large?

R: The resolution of the image extracted from nadir video camera is 2592*1952. Although the subdomain size was large, the subdomain was still contained within the boundaries of the image.

Table 1 and 2: What unit have the numbers? Is this only solar radiative forcing or total (solar + terrestrial)?

R: The units is Wm^{-2} were added. As we discussed before, we decided to remove Table 1 and 2.

Figure 4: Can you provide the parametrization equation (linear regression?) and the regression coefficients. This might be useful for other research studies.

R: As stated in the text, the parameterization was linear regression. There were hundreds of coefficients and we decided not to include the coefficients in the text but make them available in the supplementary materials (see "s2_surface-albedo-coefficients.h5"). We will upload these regression coefficients in a data file and shared it as supplementary material of this paper.

Figure 8: a) There are data points behind the text. c) Add a legend. And use two labels c) and d) for the left and right panel. In the caption there is a typo in "MOODIS".

R: We relocated the text label to reveal the data points and added the legend. We used two different labels (c) and (d) for the left and right panels. Thanks for noticing the typo. We corrected the typo "MOODIS".

Figure 10a: The label hides some of the data.

R: We relocated the label of legend to avoid covering the data.

Figure 10: Indicate the wavelengths used in Fig. 9.

R: We added two vertical lines in Figure 10 to indicate the wavelengths used in Figure 9.

Figure 10b: I suggest to remove the ratio here as the absolute irradiance is almost zero in the range of water vapor absorption. It could be better to show absolute differences instead of a ratio. If the comparison should be linked to the broadband irradiance, the absolute difference will be integrated and result in the difference of the broadband irradiance. Short: 5% difference at 500 nm is more important for broadband than 5% difference at 1600 nm.

R: Thanks for your suggestion. We agreed that the irradiance difference would work better than ratio when indicating the spectral contribution to the broadband bias. We replaced the ratio plot with the irradiance difference plot.

Figure 12: Why $\tau = 10000$ and not infinity? Please use τ instead of x. Also here: Do you need to include the water vapor bands wavelengths and have a y-axis down to zero?

R: We initially used a large value of τ, e.g., $\tau = 10000$, to simply the calculation. In the revised manuscript, we changed τ to infinity and used the analytic solution for the results. We also changed x to τ. No, we do not need to include the water vapor bands. We removed the results at the absorption wavelengths and zoomed in the y-axis.

Figure 13: Provide equation and coefficients of the fit. Not necessarily in the figure, but in the text.

R: Thanks for the suggestion. We added the equation and the coefficients of the fit to the text in the Appendix B (see **Line 31, Page 16**).

The Effect of Low-Level Thin Arctic Clouds on Shortwave Irradiance: Evaluation of Estimates from Spaceborne Passive Imagery with Aircraft Observations

Hong Chen[1,2], Sebastian Schmidt[1,2], Michael D. King[2], Galina Wind[3], Anthony Bucholtz[4], Elizabeth A. Reid[4], Michal Segal-Rozenhaimer[5,6,7], William L. Smith[8], Patrick C. Taylor[8], Seiji Kato[8], Peter Pilewskie[1,2]

[1]University of Colorado, Department of Atmospheric and Oceanic Sciences, Boulder, CO, USA
[2]University of Colorado, Laboratory for Atmospheric and Space Physics, Boulder, CO, USA
[3]Science Systems and Applications, Inc., Lanham, MD, USA
[4]Naval Research Lab, Monterey, CA, USA
[5]Bay Area Environmental Research Institute Sonoma, Sonoma, CA, USA
[6]NASA Ames Research Center, Moffett Field, CA, USA
[7] Department of Geophysics, Porter School of the Environment and Earth Sciences, Tel-Aviv University, Israel
[8]NASA Langley Research Center, Climate Science Branch, Hampton, VA, USA

Correspondence to: Sebastian Schmidt (sebastian.schmidt@lasp.colorado.edu)

Abstract. Cloud optical properties such as optical thickness along with surface albedo are important inputs for deriving the shortwave radiative effects of clouds from space-borne remote sensing. Owing to insufficient knowledge about the snow or ice surface in the Arctic, cloud detection and the retrieval products derived from passive remote sensing, such as from the Moderate Resolution Imaging Spectroradiometer (MODIS), are difficult to obtain with adequate accuracy – especially for low-level thin clouds, which are ubiquitous in the Arctic. This study aims at evaluating the spectral and broadband irradiance calculated from MODIS-derived cloud properties in the Arctic using aircraft measurements collected during the Arctic Radiation-IceBridge Sea and Ice Experiment (ARISE), specifically using the upwelling and downwelling shortwave spectral and broadband irradiance measured by the Solar Spectral Flux Radiometer (SSFR) and the BroadBand Radiometer system (BBR). This starts with the derivation of surface albedo from SSFR/BBR, accounting for the heterogeneous surface in the marginal ice zone (MIZ) with aircraft camera imagery, followed by subsequent inter-comparisons of irradiance measurements and radiative transfer calculations in the presence of thin clouds. It ends with an attribution of any biases we found to causes, based on the spectral dependence and the variations of the measured and calculated irradiance along the flight track.

The spectral surface albedo derived from the airborne radiometers is consistent with prior ground-based and airborne measurements, and adequately represents the surface variability for the study region and time period. Somewhat surprisingly, the primary error in MODIS-derived irradiance fields for this study stems from undetected clouds, rather than from the retrieved cloud properties. In our case study, about 27% of clouds remained undetected, which is attributable to clouds with an optical thickness of less than 0.5. The radiative effect of those clouds that were detected was -40 Wm^{-2} (-39 Wm^{-2}) above (below) the cloud layer, and the optical thickness from the MODIS "1621" cloud product was consistent with the reflected and transmitted irradiance observations.

We conclude that passive imagery has the potential to accurately predict shortwave irradiances in the region if the detection of thin clouds is improved. Of at least equal importance, however, is the need for an operational imagery-based surface albedo product for the polar regions that adequately captures its temporal, spatial, and spectral variability to estimate cloud radiative effects from space-borne remote sensing.

1 Introduction

Understanding the warming of the Arctic necessitates an understanding of the radiative impact of clouds and surface albedo, especially at the surface where the interaction with the cryosphere occurs (Curry et al., 1996; Shupe and Intrieri, 2004). Clouds cool the surface in the shortwave (SW) wavelength range by reflecting solar radiation and warm the surface in the longwave (LW). Low-level, liquid-bearing clouds have recently received special attention because they significantly contributed to the 2012 enhanced Greenland ice melt (Bennartz et al., 2013). When they are optically thin (LWP smaller than 20 gm^{-2}), their SW cooling effect is small because they do not reflect much sunlight, especially when the surface is already bright. In the LW, on the other hand, their emissivity increases rapidly with the liquid water path (LWP), making them blackbodies and warm the surface especially if they are at a low altitude. For larger LWP, the SW cooling eventually dominates as the cloud becomes more reflective.

Valuable data on Arctic clouds has been collected by ground-based observations over the past few decades (Curry et al., 1996, Shupe et al., 2011), but they are limited in spatial coverage and needed to be augmented by additional observations, especially from space-borne remote sensing measurements to help gain meaningful insights of cloud radiative effects in the Arctic as a whole.

Hartmann and Ceppi (2014) used the dataset from the Clouds and the Earth's Radiant Energy System (CERES) and showed that every 10^6 km^2 decrease in September sea ice extent is associated with a 2.5 Wm^{-2} increase in annual-mean absorbed solar radiation averaged over the region from 75º N to 90º N. Kay and L'Ecuyer (2013) used combined products from active and passive remote sensing and showed that during the 2007 summer, the cloud reduction and sea ice loss in the Arctic resulted in more than 20 Wm^{-2} anomalies in shortwave radiation at the top of the atmosphere (TOA). The radiation products used in these studies, e.g., CERES-EBAF (Clouds and Earth's Radiant Energy Systems - Energy Balanced And Filled, Loeb et al., 2012), 2B-FLXHR-LIDAR (Level 2B radiative fluxes and heating rates calculated from radiative transfer model by utilizing radar-lidar cloud and aerosol retrievals from A-Train satellites, Henderson et al., 2013), all rely on coincident cloud observations from the Moderate Resolution Imaging Spectroradiometer (MODIS).

MODIS is a 36-band passive imager onboard the Terra and Aqua satellites. It provides cloud optical parameters (COPs), e.g., cloud optical thickness (COT), cloud effective radius (CER), and cloud thermodynamic phase, from which irradiance can be derived. The COPs from MODIS have been used extensively in studies of cloud radiative effects (e.g., Wielicki et al., 1996; Platnick et al., 2003; Loeb and Manalo-Smith, 2005; Oreopoulos et al., 2016). Due to the lack of temperature and reflectance contrast between clouds and the underlying surface in the Arctic, detecting the clouds is challenging for passive remote sensing, especially when they are thin and occur at a low level. Liu et al. (2010) showed that the MODIS cloud detection algorithm performs better over the ocean than over the ice. The traditional cloud retrieval algorithm (Nakajima and King, 1990) retrieves COT and CER from the reflectance at two channels, one where clouds do not absorb (660, 860, or 1240 nm), and one where cloud drops are weakly absorbing (1630 or 2130 nm). Over snow and ice, the surface albedo is already high in the visible and near-infrared (leaving little dynamic range for cloud remote sensing of optical thickness) and varies regionally and temporally (leading to uncertainties in the retrieval products). This, in combination with low-sun conditions, makes it difficult to obtain accurate cloud optical properties from passive remote sensing. To improve the reliability of MODIS cloud retrievals in the Arctic, an algorithm has been developed that uses two shortwave-infrared bands of 1630 nm and 2130 nm, where snow and ice are relatively dark (Platnick et al., 2001; King et al., 2004). However, the surface albedo varies with surface type even for these bands, and the operational algorithm assumes constant values obtained from a climatology based on 5 years of Terra/MODIS data (Moody et al., 2007).

In addition to the COPs themselves, the snow/ice surface albedo also plays an important role in determining the cloud radiative effect and radiation energy budget in the Arctic (Curry et al., 1995; Shupe and Intrieri, 2004). The surface albedo changes significantly from the visible to the near-infrared wavelength range (Wiscombe and Warren, 1981; Brandt et al., 2005) with different spectral dependence depending on the surface conditions (e.g., snow and ice). Inhomogeneous surface conditions such as

floes of partially snow-covered ice, varying snow depth and snow grain size, and surface topography (e.g., sastrugi), all affect the spectral shape and magnitude of the surface albedo. To improve the understanding the inhomogeneous Arctic surface and the spectral dependence of surface albedo, spectral surface albedo measurements for snow and ice have been collected during ground-based field experiments in the polar regions (e.g., Perovich et al., 2002; Brandt et al., 2005). In addition, Perovich et al. (2002) showed that different surface types, e.g., ice, ponds, leads etc., can be identified from aerial camera images through an image processing software. Moreover, a spectral surface albedo model has been developed for different Arctic surfaces such as white sea ice, snow, and melting ponds on sea ice (Malinka et al., 2016 and 2018). However, an operational surface albedo product based on space-borne observations is still not available for the polar regions – in contrast to the land surfaces of the lower latitudes (Strahler et al., 1999).

Finally, accurate knowledge of the water vapor is also important, even in the shortwave (as we will show in this paper). In summary, the challenges for deriving shortwave irradiance from passive remote sensing are (a) inaccurate detection of clouds and cloud optical property retrievals over snow or ice surfaces; (b) lack of accurate surface albedo as a constraint in the radiative transfer model (RTM); (c) insufficient knowledge about the water vapor profile.

The aim of this paper is to use aircraft radiation measurements collected during the NASA Arctic Radiation – IceBridge Sea & Ice Experiment (ARISE, Smith et al., 2017) to evaluate irradiance as derived from coincident satellite imagery, and to investigate the causes of any biases. In the first step, the spectral snow surface albedo was derived from upwelling and downwelling irradiance measurements, accounting for partially snow-covered scenes by the snow fraction estimated from aircraft camera imagery. In the second step, we used an RTM to calculate the upwelling and downwelling broadband and spectral irradiance at flight level, incorporating the MODIS-derived COPs and spectral surface albedo derived from the aircraft measurements as inputs.

The calculated irradiances were then compared with the measured broadband and spectral irradiance pixel by pixel for two cases – above-cloud and below-cloud. Section 2 describes the data and method used in this study. Section 3 provides the results and discussions for the measured spectral surface albedo, as well as for the comparisons between irradiance calculations and measurements. Conclusions are drawn in Section 4.

2 Data and Methods

ARISE was a NASA airborne measurement campaign to study snow and ice properties in the Arctic marginal ice zone (MIZ) in conjunction with cloud microphysics and radiation (Smith et al., 2017). The NASA C-130 aircraft was instrumented with shortwave and longwave radiometers, described in this section, along with cloud microphysics probes, aerosol optical properties instruments, and snow and ice remote sensors. The experiment was based at Eielson Air Force Base near Fairbanks, Alaska, from 2 September to 2 October 2014, to capture the September sea ice minimum. In the Arctic, overpasses of polar-orbiting satellites are fairly common. ARISE targeted multiple overpasses of MODIS and CERES on Aqua, Terra, or VIIRS on Suomi NPP on almost every flight. One of the primary objectives of ARISE was to validate irradiance (or flux densities) derived from CERES-MODIS observations with aircraft radiation measurements. Figure 1 shows two science flights on 11 September and 13 September that sampled above- and below-cloud conditions, respectively. These flights include so-called "lawnmower" patterns, a series of parallel flight legs laterally offset by about 20 km. They were specifically designed for ARISE to sample one or two 100 × 100 km^2 grid boxes per flight with a sufficient number of coincident CERES footprints (each with a 20-km diameter at nadir), as to acquire statistically significant above- or below-cloud aircraft measurements for the validation of CERES-MODIS derived irradiance.

Comparing the aggregated data from ARISE directly with the CERES-MODIS flux products within the grid box, e.g., using histograms, is challenging because of the heterogeneity of the scenes in terms of surface albedo, cloud conditions, and

changing solar zenith angle. Therefore, in this paper, we instead compare aircraft observations directly (pixel by pixel) with calculations based on MODIS cloud retrievals along the flight track. The comparison of the aggregated data with CERES-MODIS products is done in a separate publication; we do not use CERES in our analysis because its large footprint does not lend itself to a direct comparison with aircraft data in a heterogeneous environment.

The first step is to merge observations of the broadband shortwave irradiance from the BroadBand Radiometer system (BBR, details in Section 2.1) and of the spectral shortwave irradiance from the solar spectral flux radiometer (SSFR, details in Section 2.2). This merged product combines the high radiometric accuracy and high-fidelity angular response from BBR with the spectral resolution from SSFR, and is referred to as "SSFR-BBR" data. From these data, the surface albedo is derived for low-level legs under clear-sky conditions. To account for the heterogeneous surface (dark ice mixed with snow-covered ice), the surface albedo is acquired as a function of snow fraction, which is estimated from images of a downward-looking video camera (Section 2.3; details on the snow-cover dependent surface albedo derivation in Section 3.1). Finally, atmospheric profiles and reanalysis data (Section 2.4) along with MODIS cloud products are used to calculate all-sky spectral and broadband irradiances along the flight track (Section 2.5), for subsequent comparison with the observations in Sections 3.2 and 3.3.

2.1 BroadBand Radiometer System (BBR)

The BBRs deployed during ARISE are modified CM 22 Precision Pyranometers from Kipp & Zonen (Bucholtz et al., 2010). The BBR included downward-looking and upward-looking sensors. The radiometers were fix-mounted on the aircraft and measured upwelling and downwelling broadband irradiance (unit: W m^{-2}), that is, the spectrally integrated irradiance from 200 nm to 3600 nm. To account for the change of sun-sensor geometry due to aircraft attitude (pitch and roll), a software attitude correction (Long et al., 2010) was applied to the BBR data. In addition, a sunshine pyranometer (SPN-1) was flown to measure diffuse and global radiative fluxes (Badosa et al., 2014; Long et al., 2010). The SPN-1 radiometer was originally intended for ground-based use, but is suited for airborne measurements of global and diffuse radiative fluxes because it does not have any moving parts, unlike traditional instruments such as the Multifilter Rotating Shadowband Radiometer (MFRSR). Smith et al. (2017) provide mission-specific details on both instruments. The BBR has a reported uncertainty of 3% (Smith et al., 2017).

2.2 Solar Spectral Flux Radiometer (SSFR)

To attribute discrepancies between satellite-derived irradiance and airborne observations to causes such as erroneous water vapor, cloud properties, or three-dimensional radiative transfer effects, spectrally resolved measurements are needed (Schmidt and Pilewskie, 2012). SSFR is a moderate resolution flux spectrometer built at the Laboratory for Atmospheric and Space Physics (LASP, University of Colorado Boulder). It is an updated version of the heritage spectrometer system originally developed at NASA Ames (Pilewskie et al., 2003). The SSFR radiometer system consists of two spectrometers for each viewing direction (zenith and nadir): 1) a Zeiss grating spectrometer with a Silicon linear photodiode detector array covering a wavelength range from 350 nm to 950 nm and 2) a Zeiss grating spectrometer with an InGaAs linear photodiode detector array covering a wavelength range from 950 nm to 2150 nm. The spectral resolution of the Silicon channels is 6 nm with a sampling of 4 nm. For the InGaAs channels, the spectral resolution is coarser – 12 nm with 6 nm sampling. From the SSFR measurements, spectral albedo, net flux, and absorption can be derived.

SSFR is typically flown in conjunction with an Active Leveling Platform (ALP, also built at LASP), which was developed for counteracting the changing aircraft attitude to keep the zenith light collector horizontally aligned (the nadir light collector was fix mounted). This is particularly important in the Arctic, where low sun elevations lead to large systematic errors for fix-mounted

or poorly stabilized sensors (Wendisch et al., 2001). One reason is that radiation from the lower hemisphere (for example, from clouds below or at the aircraft altitude) is registered by the zenith detector when it is tilted, which leads to systematic biases that cannot be corrected. Another reason lies in the specific design of the SSFR light collectors, which are realized as integrating spheres with a circular aperture on top. They diffuse the incoming light collected by the aperture and bundle it into a fiber optics cable that transmits it to the radiometer system inside the aircraft (Schmidt and Pilewskie, 2012). The integrating sphere has an imperfect response to the incidence (polar) angle θ (Kindel, 2010), in contrast to the response of broadband radiometers such as BBR, which are closer to cos(θ) as required for irradiance. At high sun elevations, a so-called hot spot arises from a baffle that prevents light from being directly transmitted into the fiber optics. Since the response deviates significantly from cos(θ), the direct and the diffuse light need to be corrected. This is done by separating the diffuse and direct component, using radiative transfer calculations in conjunction with SPN-1 measurements (details are provided in Appendix A), and further assuming that the downwelling diffuse radiation is close to isotropic. This assumption is an approximation, which becomes invalid if parts of the lower hemisphere are in the light collector's field of view.

The light collector's angular response to the azimuthal angle also needs to be considered. Throughout the course of the mission, the zenith data revealed a dependence on the relative azimuth of the sun to the aircraft. This dependence was characterized at the end of the mission, by two calibration circles flown on 2 October. The non-homogeneous azimuthal response of the zenith light collector occurred for solar zenith angles greater than 66°. Generally, an azimuthally variable response could either be attributed to aircraft interference (e.g., by the tail and/or propellers of the host aircraft), or to the light collector itself. For the former, BBR and SPN-1 (both fix-mounted on the C-130) would also be affected. To assess their azimuthal response, the attitude-corrected BBR data (Bannehr and Schwiesow, 1993; Bucholtz et al., 2008; Long et al., 2010) was compared with the SPN-1 global irradiance data, as well as with radiative transfer calculations. This comparison revealed that in this case, aircraft interferences were minor compared to atmospheric effects (e.g., cirrus), and that only SSFR measurements, but not BBR and SPN-1, had a significant azimuthal dependence, suggesting the SSFR light collector as the source, rather than aircraft interferences. In order to determine the azimuthal dependence, the SSFR measurements were referenced to the BBR measurement[1] during the calibration circle (details in Appendix B). This azimuthal correction function (dependent on the relative azimuth angle of the aircraft and the sun) was then used for the zenith SSFR data for all research flights. After azimuthal correction, the SSFR downwelling irradiance was scaled to BBR using the method described in Appendix D. It is in this sense that the BBR and SSFR measurements are merged. By using BBR, SPN-1, and SSFR in such a way, the redundancies between the instruments were used to capitalize on the strengths of the individual instruments (BBR: un-biased angular response and high radiometric accuracy; SPN-1: diffuse/global separation; SSFR; spectral resolution for sub-range of BBR and SPN-1). The SSFR nadir signal was also referenced to the BBR data in a similar manner (see Appendix D) because BBR has the better angular response, whereas SSFR provides spectral resolution. The details about the merging method and the uncertainties of the merged irradiance product are provided in Appendix D.

The angular dependence of SSFR was verified in the laboratory. In addition, wavelength and radiometric calibrations were performed before and after the mission. The wavelength calibrations ensured spectral accuracy by referencing the SSFR measurements to several line sources. The primary radiometric calibration, performed with a NIST-traceable calibrated lamp, links SSFR measured digital counts to spectral irradiance. The radiometric calibration was also transferred to a so-called secondary radiometric field standard, which monitored the stability of the radiometers throughout the mission.

[1] Since BBR has a near-ideal angular response, the attitude correction with respect to the polar angle can be performed by software as long as data are limited to small deviations from level. By contrast, SSFR with its non-ideal angular response requires an active leveling platform.

2.3 Imagery from Downward-Looking Video Camera

A downward-looking video camera (referred to as "nadir camera") is often included as a standard payload on NASA aircraft. It is a standard, commercially available video camera and typically records scenes for context only and is not radiometrically or geometrically calibrated. Despite this shortcoming, the videos recorded by the nadir camera are used for quantitative image analysis. From the video, we first extract image frames with an average rate of 2 Hz (2 frames per second). The extracted image has a pixel resolution of 2592 (width) ×1944 (height). To co-register the aircraft nadir imagery with the measurements from other instruments, the times for the individual image frames are needed, but the image frames themselves did not contain a digitally stored time. They include a timestamp located at the lower left side that contains time information, and we used Optical Character Recognition (OCR) to retrieve the time from this information.

In the second step, the nadir camera imagery was used to quantify the fractional snow coverage. The snow fraction, which is the fraction of bright pixels of the image, was estimated. To this end, the image was converted from RGB (red, green, and blue) into grayscale by

$$Gray = 0.299R + 0.587G + 0.114B \quad (1)$$

for each pixel. The weights come from standardized encoding recommendations for television (referred to as BT.601[2]). Another choice would have been to use a single-color channel, or even use the color information to distinguish surface types, but that was not necessary here. For more sophisticated imagery analysis, see Perovich et al. (2002).

One issue of the nadir camera imagery was the darkening effect from the center to the edge of its field of view, which is known as the vignette effect. To compensate, the brightness of the image was linearly increased from edge to center through an image blending and interpolation technique by Haeberli and Voorhies (1994):

$$out = (1 - \beta) \times Black + \beta \times Gray \quad (2)$$

where *Black* is a black image with the same dimensions as Gray, and β is the image blending factor, a 2D matrix with increasing values of 1.1-1.5 from the image center to the edge. The operator "×" denotes element-by-element multiplication. To avoid the vignetting extremes in the corners, only the imagery within a concentric sampling area was used to derive snow fraction (left panel of Fig. 2a). The key step of the snow fraction detection algorithm is the separation of dark versus bright pixels. To do this, an adaptive thresholding technique was applied. It is an approach for handling an image with unevenly distributed intensities by dividing the image into subimages and assigning different thresholds for each of the subimages (Gonzalez et al., 2002). The details of the adaptive thresholding are described in Appendix C. The snow fraction is then estimated by

$$Frac = \frac{N_{bright}}{N_{total}} \quad (3)$$

where N_{bright} is the number of pixels above the variable threshold, and N_{total} is the total number of pixels within the sampling area. The imagery and detection results are illustrated in Fig. 2a, whereas Figure 2b shows the simultaneously measured upwelling and downwelling spectral flux. The uncertainties associated with the estimated snow fraction are discussed in Appendix D.

[2] https://www.itu.int/dms_pubrec/itu-r/rec/bt/R-REC-BT.601-7-201103-I!!PDF-E.pdf

2.4 C-130 Thermometer and Hygrometer and Modern-Era Retrospective analysis for Research and Applications version 2 (MERRA-2)

The NASA C-130 aircraft was equipped with a thermometer and a hygrometer to measure air temperature and relative humidity, but it did not carry a dropsonde system. Figure 3b shows the profiles derived from the C-130 during a descending leg from 19:31:14 (altitude: 6.447 km) to 19:50:05 (altitude: 0.258 km) on 13 September, 2014. Due to a malfunction of the hygrometer on 11 September, 2014, no water vapor profile from the C-130 is available on this day. Instead (Figure 3a), we used the temperature and water vapor content profiles from MERRA-2, which is an atmospheric reanalysis dataset from NASA (Bosilovich et. al., 2015). MERRA-2 (M2I3NVASM) provides 3-hourly assimilated 3D meteorological fields (dimensions: 576 in longitude; 361 in latitude; 72 pressure levels from 985 hPa to 0.01 hPa). The comparison of the in-situ profiles and MERRA-2 (Figure 3b) shows good agreement, although the reanalysis does not reproduce the details of the vertical profile. A more systematic comparison of reanalysis and in-situ data from ARISE is done by Rozenhaimer et al. (2018) and is not the focus of this paper. The observations reveal much drier and slightly colder conditions than captured in the subarctic climatology from Anderson et al. (1986), referred to here as AFGL. Nevertheless, we used the climatology above 6.5 km to provide complete temperature and water vapor profiles from 0 to 120 km, after rescaling them to the observed temperature and water vapor values at 6.5 km. The constructed atmospheric profiles were then used in the RTM (described in the next subsection) to obtain irradiance calculations.

2.5 Radiative Transfer Calculations based on MODIS Cloud Products

The publicly available pixel-level MODIS cloud products (MOD/MYD06, collection 6.1), which are provided in 5-minute granules (Platnick et al., 2017), are used in this study. The MODIS cloud product includes COPs such as COT, CER, and cloud thermodynamic phase, which are essential parameters for calculating cloud radiative effects. As described before, the MODIS COT and CER are retrieved simultaneously using a bi-spectral reflectance method (Nakajima and King, 1990). To minimize the influence of the surface on cloud retrievals, the 1630 nm and 2130 nm bands are used since the snow and ice surface are relatively dark at those two bands (Platnick et al., 2001; King et al., 2004). These retrievals are included in the MOD/MYD06 files and will be referred to as the "1621" cloud product. Limited in-situ observations suggested that the clouds consisted primarily of liquid water, and the MODIS cloud phase product showed less than 2% of ice clouds along the flight track. Therefore, the clouds were assumed to be liquid.

The MODIS "1621" product includes COPs for cloudy and partially cloudy conditions. The latter are denoted as "PCL" in the MODIS data variable name. The product was extracted along the flight track and then input into a radiative transfer model (RTM) to calculate spectral and broadband irradiance at flight level. A 1-D RTM (libRadtran version 2.0.1, Emde et al., 2016) was used for the calculations. It requires the following inputs:

1) Day of the year (for accurate Sun-Earth distance);
2) Atmospheric profile; here, the subarctic summer atmospheric profile from Anderson et al. (1986) along with:
    a) Water vapor content profile from MERRA-2 for 11 September and from the C-130 hygrometer for 13 September, 2014;
    b) Temperature profile from MERRA-2 for 11 September and from the C-130 thermometer for 13 September, 2014;
3) Solar zenith angle;
4) Wavelength;
5) Surface albedo at the specified wavelength (see Section 3.1);

6) Slit functions (also known as instrument line shape), which describe the bandpass function of the spectrometer. Here, SSFR slit functions as measured in the laboratory are used (full width at half maximum (FWHM) of 6 nm for the Silicon channels and FWHM of 12 nm for InGaAs channels);
7) Cloud optical thickness, and cloud effective radius; here, from MODIS-COPs;
8) Phase functions; here, from Mie calculations distributed with libRadtran;
9) Output altitude grid; here: only at the aircraft flight level.

The RTM uses a solar spectrum with 1 nm resolution as solar source at TOA (Kurucz, 1992). The Discrete Ordinates Radiative Transfer Program (DISORT, Stamnes et al, 1988) is used as the radiative transfer solver. LOWTRAN 7 (Pierluissi and Peng, 1985) is used for the molecular absorption parameterization. The cloud layer altitude was set to 0.8 km to 1.0 km for 13 September according to the water vapor profile from the aircraft hygrometer. Since the hygrometer data was not available for 11 September and the cloud layer could not be identified from the temperature profile, the mean of cloud top height from MODIS and a cloud geometrical thickness of 0.2 km were used in the calculations. The RTM output includes downwelling (global and direct) and upwelling irradiance at the specified wavelengths and output altitude (in this case, at the flight altitude). The cloud layer location and flight level altitude range were indicated in Fig. 3. The wavelength range of the calculations is set to 200 to 3600 nm, which encompasses both BBR and SSFR.

3. Analysis and Results

This section shows the results for the spectral surface albedo derivation from the irradiance data and the aircraft camera imagery, as well as the comparison of broadband and spectral irradiance between aircraft measurements and radiative transfer calculations. The spectral mixed-scene surface albedo parametrization (described first) is used as input to the RTM calculations in the subsequent comparisons with broadband and spectral irradiance observations. Finally, any biases are attributed to different sources based on their spectral fingerprint.

3.1 Spectral Surface Albedo

From the simultaneous measurements of spectral downwelling and upwelling irradiances ($F(\lambda)^{\downarrow}$ and $F(\lambda)^{\uparrow}$), the surface albedo

$$\alpha(\lambda) = \frac{F(\lambda)^{\uparrow}}{F(\lambda)^{\downarrow}} \quad (4)$$

can be derived through atmospheric correction (Appendix E) from low near-surface legs under clear-sky conditions. Clear-sky measurements were a rare occurrence because low-level clouds were ubiquitous. In this study, we used clear-sky measurements of SSFR-BBR from 20:00:26 UTC to 20:10:51 UTC on 13 September (referred to as "0913-clear-sky"). A time-synchronized video of the flight is provided as supplementary material (S1 "s1_flight-video_20140913-clear-sky.mp4"). This video shows that the Arctic surface varied significantly – from snow scenes to scenes with a large amount of dark ice. Clear-sky scenes (no clouds above or below) were identified from the forward and nadir cameras. During the "0913-clear-sky" case, the aircraft flew at an altitude at around 240 m.

To make full use of the direct measurements of the spectral surface albedo from SSFR-BBR, we parameterized the surface albedo by snow fraction, which can be estimated from the nadir camera imagery (described in Section 2.3). The parameterization was done through a data aggregation technique that combines collective measurements in a partially snow-covered environment. Figure 4 shows the surface albedo at 640 nm, 1240 nm, and 1630 nm plotted versus the snow fraction. The uncertainties of the

surface albedo and snow fraction are indicated as vertical and horizontal error bars, respectively (details are provided in Appendix D). The data showed that linear regression can be used to establish a simple relationship between snow fraction and albedo, assuming that each observed spectrum is a mixture of only two so-called end-members: the spectral albedos of a dark and a bright surface. These end-members can vary depending on the local conditions. For example, the dark component can either be open ocean or young ice. The bright component can either be thick ice or a snow-covered surface. The resulting spectral surface albedo for a mixed sampling region is established through the slopes s_λ and intercepts i_λ of the linear fit, with the snow fraction SF ranging from 0 to 1 as the independent variable:

$$\alpha_\lambda = i_\lambda + s_\lambda SF \quad (5)$$

The linear regression coefficients (i_λ and s_λ) and associated uncertainties were obtained through orthogonal distance regression (Boggs and Rogers, 1990) for all the SSFR wavelengths except for the water absorption bands, and those less than 350 nm or greater than 1800 nm because of a low signal-to-noise ratio. We provided the coefficients as a supplementary material (see S2 "s2_surface-albedo-coefficients.h5"). This simple surface albedo parameterization has obvious drawbacks; for example, the implicit linear-mixing assumption, the variability of the end-members, and data sparsity of the individual end members (in the example in Fig. 4, snow fractions below 0.6 rarely occur).

The snow spectral end-member (snow fraction of 1) of the mixed-scene spectral surface albedo (referred to as "2014-09-13 surface albedo") is shown in Fig. 5. The error bars of the surface albedo are larger in shortwave than in the near-infrared. As expected, the surface albedo is high in the shortwave range from 400 to 900 nm and decreases in the near-infrared. The SSFR-BBR derived albedo spectra resemble the ground-based measurements of thick snow over ice near Davis Station, Antarctica (Brandt et al., 2005), and they are also close to spring-time aircraft measurements near Barrow (Alaska, Lyapustin et al., 2010). Figure 5 also shows the surface albedo with zero snow fraction. As pointed out above, snow fractions below 0.6 were extremely rare during "0913-clear-sky". Nevertheless, the mixed-surface data, extrapolated to 0 snow fraction, compares surprisingly well to ground-based measurements of young gray ice, taken during the Australian National Antarctic Research Expeditions (ANARE) in 1996 (Warren et al., 1997). The spectra shape of the surface albedo at 0 snow fraction (along with the nadir camera imagery from S1) suggests that during the sampled time period, the dark pixels were ice at various freezing states instead of open ocean. As mentioned above, the binary representation of surface types oversimplifies the actual mixture of ice and snow, but is adequate to serve as surface albedo input for the RTM to constrain the irradiance calculations over mixed surfaces, which is our primary goal here.

3.2 Broadband Irradiance Comparison

In this section, we show broadband irradiance comparisons between SSFR and BBR measurements and MODIS-COPs based RTM calculations at aircraft flight level for an above-cloud case (referred to as "0911-above-cloud") and a below-cloud case (referred to as "0913-below-cloud"), collected by the research flights on 11 September and 13 September, respectively.

The RTM irradiances were calculated for wavelengths from 200 nm to 3600 nm. Since the SSFR-BBR derived surface albedo described in previous subsection was not available at wavelengths shorter than 350 nm, in gas absorption bands, and for wavelengths greater than 1800 nm due to a low signal-to-noise ratio, several techniques were applied to fill in the surface albedo spectra (details in Appendix F). For both the "0911-above-cloud" and "0913-below-cloud" cases, the surface albedo along the flight track was calculated from *SF* as driving parameter to Equation (5). For "0913-below-cloud", *SF* was determined from the camera imagery; for "0911-above-cloud", that was not possible because the surface was not visible through the clouds, and *SF* was instead set to a constant value of 76.4%. This value was obtained by modifying *SF* in Equation (5) to obtain a set of spectral surface

albedo that brings the upwelling irradiance calculations at 1640 nm in agreement with the observations for the clear-sky baseline of this case[3]. It should be noted that the observed albedo is the blue-sky albedo (direct beam and diffuse light conditions), whereas the albedo required for the cloud cases is the white-sky albedo (diffuse light only). The difference between the two is discussed by Gardner and Sharp (2010). In addition, it is assumed that the simple parameterization as expressed in Equation (5) holds for the whole study region. This is justified because the measurements occurred in the same general area. Figure 6 shows the surface albedo calculated for *SF*=76.4% for "0911-above-cloud". Comparing with dry- and wet-season surface albedo climatology from Kay and L'Ecuyer (2013), the wet-season climatology agrees well with SSFR-BBR derived surface albedo in the shortwave (wavelength less than 900 nm) except for wavelength 660 nm, where climatology has a higher surface albedo. In the shortwave near-infrared (wavelength greater than 900 nm) however, the dry-season climatology agrees better with SSFR-BBR derived albedo than wet-season. It is worth noting that the surface albedo assumed in MODIS 1621 cloud retrievals (Platnick et al., 2018) agrees with the surface albedo we obtained from SSFR-BBR.

Figure 7 and Fig. 8 show the broadband irradiances from SSFR-BBR, BBR, and the calculations (Fig. 7a: downwelling; Fig. 7b: upwelling) for the "0911-above-cloud", where the aircraft was flying at an altitude around 7 km. The observed variability in the downwelling signal is due to the occurrence of cirrus above the aircraft, which is confirmed by the forward camera. The cirrus was not considered in the RTM because we did not have optical thickness information from MODIS (which does not distinguish between cirrus and low-level clouds) and because we did not pursue radiative closure study as primary purpose of this paper. For the upwelling irradiance, the MODIS-derived baseline value of 230 Wm^{-2} corresponds to locations where MODIS did not detect any clouds. It is important to note that the value of the baseline indicates the RTM calculations under clear-sky condition, which would change if a different surface albedo parameterization or a different snow fraction were used. For a *SF*=76.4%, the calculations agree with the measurements within 10%. The cloud optical thickness along the flight track (included in Fig 7b) ranges from 0.5 to 15.3, with a median of 5.7, suggesting that MODIS does not retrieve clouds with an optical thickness below 0.5. In contrast to the calculations, the measurements show a continuous variation from leg to leg, suggesting that the clouds actually extended beyond the locations where MODIS detected them. Since the SSFR/BBR sensors integrate the cosine-weighted radiances hemispherically, they do not the same field of view (FOV) as MODIS pixels. The clouds detected by SSFR/BBR but not by MODIS could therefore be caused by clouds located outside the FOV of MODIS. To take this into account, we assume a 45° FOV for the SSFR/BBR that encompasses roughly half of the irradiance signal for an isotropic radiance distribution. When the aircraft was flying at 7 km, the FOV diameter of SSFR/BBR is 7 km (indicated as horizontal bars in Figure 7b, translated into a time range using the aircraft speed). This is larger than the 1 km MODIS pixel-level product FOV. However, the results indicate that cloud portion missed by MODIS exceeds the FOV of the aircraft radiometer and therefore cannot be explained by the mismatch in the observational geometry. To further corroborate that the MODIS algorithm is indeed missing clouds, a sequence of nadir camera imagery (Fig. 7b i - iv) is considered. At close inspection, the images reveal wave patterns, suggesting the existence of thin clouds in regions where MODIS does not detect any. In this case, undetected, optically thin clouds made up more than one fifth of the points along the flight track. Fig. 7b indicates that these undetected clouds lead to an underestimation of the upwelling irradiance by 30 Wm^{-2} averaged over these pixels (>10% discrepancy). By contrast, the calculated irradiances for the locations where MODIS does detect clouds are only 10 Wm^{-2} lower than the measurements (4%), which is only slightly larger than the BBR/SSFR measurement uncertainty and can be explained either by (a) incorrect COPs (optical thickness, effective radius, or thermodynamic phase) and/or (b) inaccurate or variable surface albedo. To quantify the contributions of these effects to the total discrepancy, the spectral information from SSFR is used in the next section.

[3] See justification under 3.3 and Figure 9b. The data from 21:12:25 UTC to 21:15:35 UTC was selected as the clear-sky baseline.

After the investigation of the above-cloud case for MODIS-derived irradiance, we turn our attention to the below-cloud case – "0913-below-cloud", which relates to near-surface irradiance. The primary cloud layer consisted of stratocumulus cloud and was located between 0.8 and 1.2 km. The cloud optical thickness (indicated in Fig. 8a) ranges from 4.1 to 8.1, with a median of 5.8. A secondary cloud layer close to the surface, located below the aircraft's minimum flight altitude of 500 ft (approximately 150 m), frequently occurs due to a temperature inversion close to the surface, where leads and cracks in the ice provide the necessary moisture for their formation. These clouds also need to be considered to quantify the radiative surface budget, but they are excluded from the analysis here because the aircraft could not underfly them. As a result, only the data from 22:21:00 to 22:25:48 (minimal occurrence of the secondary cloud layer as indicated by the forward and nadir camera imagery) was selected for comparison. A time-synced video for this flight leg is provided in the supplementary materials (see S3 "s3_flight-video_0913-below-cloud.mp4"). As mentioned before, in contrast to the above-cloud case where the surface albedo was held constant in the RTM, the surface albedo variability on the below-cloud leg was considered here. Figure 8 shows the upwelling and downwelling broadband irradiance comparison between calculations and observations from SSFR-BBR and BBR. When incorporating the "13 September surface albedo" into the RTM, the upwelling irradiance calculations resemble the SSFR-BBR and BBR measurements (Fig. 8b). The calculations agreed well with SSFR-BBR and BBR when clouds were detected except for the time period before 22:22:48 UTC when the aircraft was entering the cloud field. The MODIS granule from Aqua was a snapshot of the cloud scene at 22:10, 10 minutes prior to the beginning of the flight leg. Measurement-model discrepancies for specific pixels can therefore be explained by changes of the cloud field over time. The bimodal behavior that is apparent in the time series (Fig. 8a and 8b) as well as in the histograms (Fig. 8c) stems from time periods with and without clouds in the model input. The observations show no evidence of any cloud gap – hence only one mode appears. The "cloud gaps" apparent in the satellite but not aircraft measurements could be caused by different viewing and sun-sensor geometries between the satellite and aircraft instruments. For example, tall clouds could block the direct sun beam measured by the aircraft radiometer when flying below clouds under low-sun conditions. By evaluating the fields of cloud optical thickness and radiance at 860 nm from MODIS (Figures 8e and 8f) and the supplementary flight video S3, we found that any cloud gaps are not large or frequent enough permit the direct beam to be transmitted. This leads to a smooth irradiance time series in the aircraft measurements. The gaps (circled in Fig. 8e, however infrequent, most likely at sub-grid scale for the 1 km product) do seem to cause gaps satellite retrievals. From the distance of the cloudy/clear modes, one can estimate the pixel-level bias caused by undetected clouds: 45 Wm^{-2} bias for the downwelling and 19 Wm^{-2} bias for the upwelling shortwave irradiance.

3.3 Spectral Irradiance Comparison

Although the model-measurement biases in the broadband irradiances are negligible when clouds were detected, the time series as shown in Fig. 7b do not quite match, especially for the thin parts of the clouds near the edge of a field. To diagnose the cause, we use the spectrally resolved measurements by SSFR-BBR in this section.

For the "0911-above-cloud", Fig. 9 presents the spectral upwelling irradiance comparison at 860nm and 1640nm. To put these results into context, the RTM calculations (using Equation (5) with SF=76.4%) were also performed with climatological surface albedos of the Arctic dry and wet seasons (0.85 and 0.75) for 860nm from Kay and L'Ecuyer (2013). As shown in Fig. 9a, the baseline of the clear-sky RTM calculations varied significantly with surface albedo. The clear-sky measurements from 21:12:25-21:15:35 UTC are slightly below the SF=76.4% baseline calculation for 860 nm, and above for other times. It is impossible to tell whether the variability at this wavelength stems from surface albedo variability or from undetected clouds. For 1640

nm (Fig. 9b), however, the clear-sky baseline is much more defined and less variable, which is why we determined *SF* based on that wavelength.

Since any inaccuracies in the spectral surface albedo will propagate into model biases for both cloudy and clear-sky conditions, an operational surface albedo retrieval in the Arctic would be highly desirable. In this context, it is important to note that the small broadband model-measurement discrepancy of 8 Wm^{-2} from Fig. 7 is only achieved when the SSFR-BBR derived surface albedo is used in the RTM calculations; when using a climatology instead, it would be larger. In other words, in absence of an operational product, the surface albedo variability dominates the uncertainty in clear- and cloudy sky irradiance calculations.

At 1640 nm (Fig. 9b), there is good model-measurement agreement for the clear-sky baseline and for cloudy pixels that MODIS detects. That is because snow is dark in the shortwave infrared, and because MODIS COPs in the Arctic are primarily based on these wavelengths. Because of the obvious distinction between cloudy and clear pixels in the measurements and calculations, it is possible to estimate the fraction of partially or fully cloudy pixels that are not detected by MODIS. Of all pixels along the flight leg with a MODIS-COD below the detection threshold of 0.5 (i.e., "clear"), 27% (highlighted in green) are actually cloudy where MODIS cloud detection algorithm identified as clear-sky. One interesting finding from the broadband irradiance comparison (Fig. 7b) is that the calculations are low-biased relative to the observations. However, from the spectral comparison (Fig. 9), the calculations have larger/similar values than the SSFR measurements at 860 nm/1640 nm. To reconcile the apparently contradictory results, we use the full spectrum from the calculations and observations at 21:24 UTC on 11 September, when the broadband calculation indicates a 6 Wm^{-2} low bias.

Figures 10a and 10b show the spectral upwelling irradiance from the RTM calculations and from the SSFR-BBR measurements, as well as the difference between RTM and SSFR-BBR. In addition to the RTM calculations with atmospheric profiles from MERRA-2 (referred to as RTM_{MERRA}), we provided the calculations with the atmospheric profile climatology (AFGL subarctic summer, Anderson et al., 1986, referred to as RTM_{AFGL}). The agreement between RTM_{MERRA} and SSFR-BBR in the water vapor absorption bands indicates that MERRA-2 is sufficient to prescribe the water vapor content in the calculations. The broadband irradiance difference between RTM_{MERRA} and RTM_{AFGL} due to water vapor is 13.5 Wm^{-2}. Outside of the gas absorption bands, the calculations agree with the measurements at wavelengths smaller than around 850nm, but are slightly low-biased at near-infrared wavelengths. Spectral discrepancies are caused by the use of inaccurate 1) surface albedo 2) cloud optical parameters, some of which compensate each other in the broadband integral. Such error compensation may lead to an improved model-measurements agreement for the "wrong reasons"; therefore, validation efforts should include spectrally resolved measurements.

So far, the analysis did not reveal whether the observed model-measurement discrepancies are due to biases in the COPs or in the surface albedo. Figures 11-12 are an attempt to disentangle both sources of uncertainty despite the limited number of observations during ARISE. Figure 11 shows the ratio between modeled (labeled "RTM") and measured ("SSFR-BBR") upwelling broadband irradiance at flight-level as a function of the retrieved COT for the collection of cloudy pixels from 11 September. At large COT, clouds dominate the upwelling irradiance, whereas the surface dominates in the limit of zero COT (as stated above, the retrieved minimum is 0.5). The ratio of RTM/SSFR-BBR can be used to indicate how biased the surface albedo is in the RTM when COT is approaching to 0 and how biased the cloud optical properties are when the COT approaches large values. The data reveal a functional relationship between *COT* and the RTM/SSFR-BBR ratio. An exponential fitting of

$$r = a - e^{b \cdot COT + c} \quad (6)$$

is used to parameterize the upwelling irradiance ratio as a function of *COT*. The black curve in Fig. 11 suggests that the surface albedo in the calculations is biased low by about 8%, whereas almost no bias is detectable in the cloud properties (a of ~1.01). Figure 12 shows the spectral fits for the wavelengths between 350 and 1800nm. Two spectra are calculated: the spectrum of the ratio when $COT = 0$ (denoted as $r_0(\lambda)$), corresponding to cloud-free conditions; and the spectrum of ratio at infinite *COT* (denoted

as $r_\infty(\lambda)$), corresponding to cloudy conditions. The $r_0(\lambda)$ spectrum (red) is consistently lower than 1.0 at short wavelengths (< 1300 nm) and slightly greater than 1.0 for wavelengths longer than 1500 nm. This suggests that the surface albedo is underestimated for the shorter wavelengths and overestimated for the longer wavelengths. Since changing the snow fraction will only increase or decrease surface albedo for all wavelengths, simply changing the snow fraction does not improve the agreement for both long and short wavelengths. As mentioned before, the albedo we used in the RTM is so called blue-sky albedo, which differs from the white-sky albedo that captured by the measured upwelling irradiance under cloudy condition. However, the spectral shape of the two ratios in Figure 12 does not suggest that this had an impact (one would have expected a molecular scattering signature for the shortest wavelengths). Instead, the discrepancies could be caused by the physical changes of the surface, different sun angles, and/or instrument performance changes. The $r_\infty(\lambda)$ spectrum (blue) oscillates around 1.0 for the shorter wavelengths and is consistently larger than 1.0 for longer wavelengths, which suggest that the retrieved effective radius is slightly biased. Unfortunately, owing to limited sampling time, the below-cloud flight (13 September) leg does not lend itself to any conclusions from a cloud transmittance perspective since it is not the same cloud field as on 11 September. In future flight campaigns, coordinated above- and below-cloud legs will furnish more information on bias analyses than possible from ARISE.

4 Conclusions

In this paper, we used aircraft observations to validate shortwave irradiance derived from satellite passive imagery (MODIS) of low-level cloud fields. This was done with two consecutive flights from the NASA ARISE campaign, which sampled the radiation below and above a cloud field in a similar location of the MIZ. Such validation studies are especially important in the Arctic because observations from the surface are sparse. Despite their limitations, passive imagery products are one of the essential data sources for observationally-based estimates of the surface radiative flux under cloudy conditions, which necessitates a quality assessment of cloud detection and the derivation of cloud optical parameters for a variety of specific cloud and surface types as well as surface angles. In addition, accurate knowledge of the surface albedo and of the water vapor vertical distribution is required to derive the net fluxes at the surface, above the cloud layer, and at the top of atmosphere. The two cases analyzed here only focused on one region with one specific surface and cloud type, but this allowed developing a validation approach that can help answer specific questions such as:

1. What is the reliability of passive imagery cloud detection in the MIZ and over solid snow-covered regions?
2. How much do undetected clouds bias imagery-derived irradiance, especially at the surface?
3. What is the relative magnitude of irradiance errors caused by undetected clouds, biased cloud properties, incorrect surface albedo parameterization, and water vapor?

This paper sheds some light on these questions using the combined measured broadband and spectral irradiance in the study region, but these results are far from representative for the Arctic as a whole. To gain a statistically based understanding, validation data from multiple experiments will have to be combined. By aggregating data from multiple missions, it should be possible to answer more general questions, which a single case study cannot address:

- Do existing cloud climatologies from space-borne passive imagery observations accurately reproduce the frequency of low-level optically thin clouds over different surface types?
- Do existing climatologies of surface albedo capture the spatial and temporal variability sufficiently to keep errors in the derived all-sky irradiance and cloud radiative effects to an acceptable level?

It is unclear what “acceptable” would mean for the second question, but our study showed that the actual surface albedo deviates from commonly used climatologies. Throughout the Arctic, inaccurate knowledge of the surface albedo and its variability will lead

to an inaccurate estimation of cloud radiative effects and net surface fluxes, even under clear-sky conditions. This is especially important in the visible part of the spectrum where most of the shortwave energy resides, and where the albedo of different surface types (ice, fresh and old snow) varies significantly. Of course, knowledge of the near-infrared variability of snow and ice albedo (via grain size) is also important because it affects the accuracy of imagery-derived cloud products.

To capture the spatial and spectral variability of the surface, we developed a data aggregation technique that combines collective measurements in a partially snow-covered environment into one spectral surface albedo dataset that is parameterized by snow fraction ("binary" representation of the radiative surface properties). The dataset we obtained agrees with ground-based measurements for the two extremes (called spectral end-members): snow and thin ice. In our case, ice-free open ocean was radiatively insignificant, and the two end-members were sufficient to represent the surface variability. In more complex, more general cases, more end-members will be required.

In assessing the relative magnitude of different errors (question 3 above), we found that undetected clouds have the most significant impact on the imagery-derived irradiance. In the case studied here, MODIS did not detect clouds below a threshold of 0.5 in optical thickness, even when including partially cloud-covered pixels. For the above cloud case, this led to a low bias of about 40 Wm^{-2} for the upwelling shortwave irradiance. The below cloud case was harder to interpret due to the limited data and the lack of knowledge about the irradiances at cloud top. However, the model-measurement comparison indicated a high bias of 45 Wm^{-2} in downwelling shortwave irradiance if clouds are not detected, which again suggested the undetected clouds the dominating error source. Secondary error sources are (a) surface albedo, (b) water vapor content, and (c) cloud optical properties. By using an SSFR-BBR derived surface albedo along with atmospheric profiles from aircraft measurements and MODIS-COPs in the RTM calculations, they agreed with the measured spectral and broadband shortwave irradiance within the range of uncertainties, except in regions where MODIS did not detect clouds. It should be pointed out that in absence of an operational surface albedo product, the surface albedo uncertainty by far dominates the calculated shortwave irradiance error.

While the radiation calculations at TOA can be constrained through the radiation product from satellite observations (e.g., CERES), the radiation calculations at the surface do not have such constraints. The attribution of the individual error contributions was done based on measurements from the SSFR-BBR, by distinguishing the different physical mechanisms based on their spectral dependence. Under some circumstances, the different errors compensate partially in the broadband irradiance.

Generalizing the findings from airborne studies such as these will only be possible by improving satellite remote sensing along the way, which in turn requires airborne observations for the development and validation of a new generation of cloud retrievals in the Arctic. Such retrievals will need to account for surface and cloud variability, and address the issue of undetected thin clouds. A database of spectral albedos, acquired with similar techniques as proposed here, would provide the necessary testbed for developing operational space-based retrievals for surface reflectance as available for the lower latitudes. With lower COT thresholds for cloud detection, spatially and temporally dependent surface albedo, accurate cloud retrievals even for thin clouds, passive remote sensing will significantly improve our current understanding of cloud radiative effects in the Arctic. Finally, it will be important to pursue a similar strategy for the thermal wavelength range.

Appendix

A. Diffuse/direct correction for the polar angle response

The polar angle response ("cosine response") needs to be done separately for the direct and the diffuse downwelling radiation. Therefore, these two components first need to be separated, assuming

$$DR(\lambda) = DR_{clear}(\lambda) \cdot f + DR_{cloud}(\lambda)(1-f)$$

where DR is the diffuse (to total, or global) ratio, *f* is the clear-sky fraction, and *(1–f)* is the fraction of a diffuser (clouds).

We can make the simplification $DR_{cloud}(\lambda) = 1.0$, (i.e., the radiation under clouds does not have a direct component), leading to

$$DR(\lambda) = 1 - f \cdot \left(1 - DR_{clear}(\lambda)\right) \quad \text{(A1)}$$

The SPN1 measures the broadband diffuse radio, which we denote as DR_{SPN1}:

$$DR_{SPN1} = \frac{\int_{\lambda_1}^{\lambda_2} DR(\lambda) \cdot F^{\downarrow}(\lambda) d\lambda}{\int_{\lambda_1}^{\lambda_2} F^{\downarrow}(\lambda) d\lambda} \quad \text{(A2)}$$

where λ_1 and λ_2 indicate the wavelength range of SPN1, and $F^{\downarrow}(\lambda)$ is the calculated downwelling (global) spectral irradiance from a RTM (we did not use the SSFR measurements because they only encompass a sub-range of SPN-1). Substituting Equation (A1) into (A2), we get

$$DR_{SPN1} = 1 - f \cdot \frac{\int_{\lambda_1}^{\lambda_2} F^{\downarrow}(\lambda) \cdot \left(1 - DR_{clear}(\lambda)\right) d\lambda}{\int_{\lambda_1}^{\lambda_2} F^{\downarrow}(\lambda) d\lambda} \quad \text{(A3)}$$

We can then determine *f* from

$$f = \frac{\left(1 - DR_{SPN1}\right) \cdot \int_{\lambda_1}^{\lambda_2} F^{\downarrow}_{clear}(\lambda) d\lambda}{\int_{\lambda_1}^{\lambda_2} F^{\downarrow}_{clear}(\lambda) \cdot \left(1 - DR_{clear}(\lambda)\right) d\lambda} \quad \text{(A4)}$$

and the diffuse/direct ratio can be calculated by using this value of *f* in equation (A1).

B. Azimuth response

The azimuth response of the SSFR zenith light collector was obtained using the data collected during the so-called calibration flight (2014-10-02), where the aircraft flew a circles to collect radiation measurements at different solar azimuth angles. This was done by referencing the SSFR irradiance measurements to the simultaneous BBR data, building on the fact that unlike SSFR, BBR had no discernable azimuthal dependence. The data used to determine the azimuth response had a solar zenith range of [68.24 º, 71.49 º] with an average of 70.20 º, whereas the solar zenith angle range for the above-cloud case (2014-09-11, where the azimuth correction was applied) was [68.46º to 71.89º] with the mean of 68.91º.

Since SSFR only covers part of BBR's bandwidth from 200 to 3600 nm, RTM calculations were used to fill in SSFR spectra beyond its nominal wavelength range of 350 – 2050 nm. Subsequently, the RTM-extended SSFR irradiance was spectrally integrated (referred to as F_{SSFR}). A second-order Fourier series was then applied to fit the azimuthal dependence captured by the ratio F_{SSFR}/F_{BBR}, shown in Fig. A1. It shows this ratio as a function of reference azimuth angle, defined as the azimuth angle of the sun with respect to the light collector, for which 0 degrees is defined as the aircraft flying due North. A second-order Fourier series was applied to fit the azimuthal dependence of F_{SSFR}/F_{BBR}. It constitutes SSFR's azimuthal response at this solar zenith angle, which was then used to correct SSFR's downwelling irradiance for the conditions encountered for the SSFR data collected during other research flights. The azimuth response obtained in Fig. A1 can be expressed as (with coefficients)

$$\frac{F_{SSFR}}{F_{BBR}} = 0.9460 + 0.0647 \cdot \cos\left(\frac{\phi}{180} \cdot \pi\right) + 0.0160 \cdot \sin\left(\frac{\phi}{180} \cdot \pi\right) - 0.0045 \cdot \cos\left(\frac{\phi}{180} \cdot 2\pi\right) - 0.0015 \cdot \sin\left(\frac{\phi}{180} \cdot 2\pi\right) \quad \text{(A5)}$$

where ϕ is the reference azimuth angle.

C. Adaptive thresholding

The threshold value at each pixel location of the image depends on the neighboring pixel intensities I. For a pixel located at (x, y), the threshold value $T(x, y)$ is calculated through the following steps:

1). A subdomain of size $d \times d$ is selected with (x, y) at the center of the subdomain;

2). The weighted average $C(x, y)$ is calculated for the subdomain using Gaussian weights (Davies 1990) $W(x, y)$, $C(x, y) = \sum_{i=0}^{d} \sum_{j=0}^{d} I(i, j) \cdot W(i, j)$;

3). The threshold for the pixel at (x, y) is the difference of the weighted average calculated in the previous step and a constant C_0, $T(x, y) = C(x, y) - C_0$.

d and C_0 are input parameters that can be adjusted to improve the results. In this study, d is set to 1501 and C_0 is set to 0.

D. Uncertainty estimation

1). SSFR-BBR irradiance product

For the SSFR spectral measurements, the nominal radiometric uncertainty is 5% (Schmidt et al., 2010). The nominal uncertainty of BBR measurements is 3% (Smith et al., 2017). As we described in section 2.2, we corrected the azimuthal dependence of SSFR downwelling irradiance based on the BBR measurements using the method described in Appendix B. After the correction, the SSFR downwelling and upwelling irradiances are still slightly inconsistent with BBR due to an imperfect cosine response comparing to BBR (although they agree with BBR within the range of uncertainty). In addition, the different sun-sensor geometries between the calibration flight (2 October, 2014) and the "0911-above-cloud" case mean that the azimuthal response as measured during the calibration flight does not necessarily fully apply to the case under study. In order to reference SSFR to BBR and simultaneously estimate the uncertainty of the merged product (SSFR-BBR), we applied a scaling method as shown in Fig. A2. Figures A2 (a) and (b) show the azimuthally corrected SSFR downwelling and SSFR upwelling irradiance versus BBR. The wide spread of downwelling irradiance indicates that even after applying azimuthal correction for SSFR, some residual uncertainty of the azimuthal response obtained in Appendix B remains in the SSFR measurements after the azimuthal correction. In the upwelling irradiance, the SSFR is more closely related to BBR. Figures A2 (c) and (d) illustrate how we correct for the remaining biases between SSFR and BBR and estimate the uncertainties of the SSFR-BBR product. Figures A2 (c) and (d) show the histogram of the ratio of SSFR and BBR measurements. The ratio histograms indicate a scale factor of 1.006 and 0.946 for the SSFR downwelling and upwelling, with standard deviations of 0.025 and 0.01 when referencing to BBR. The scale factors of 1.006 and 0.946 are applied as divisor to SSFR downwelling and upwelling irradiance respectively. The SSFR irradiance after scaling (referred to as SSFR-BBR) versus BBR is shown in Figures A2 (a) and (c) in green. After scaling, the SSFR-BBR and BBR achieve a better consistency. The standard deviations of 0.025 and 0.01 represent the precision for the downwelling and upwelling irradiance of SSFR-BBR. Thus, we use 2.5% (0.025/1.006*100%) and 1% (0.01/0.946*100%) as the precision estimates for SSFR-BBR downwelling and upwelling, whereas the uncertainty propagates from BBR into the SSFR-BBR product (3%).

2). Snow fraction and surface albedo

When calculating the surface albedo from SSFR-BBR using Equation (4), we use the precision as determined above because the uncertainty cancels out for the ratio between the upwelling and downwelling irradiance. The uncertainty estimate of 2.7% for the surface albedo α is then obtained through error propagation using Equation (4), where

$$\frac{u(\alpha(\lambda))}{\alpha(\lambda)} = \sqrt{\left(\frac{u(F(\lambda)^{\uparrow})}{F(\lambda)^{\uparrow}}\right)^2 + \left(\frac{u(F(\lambda)^{\downarrow})}{F(\lambda)^{\downarrow}}\right)^2} \quad \text{(A6)}$$

The uncertainty of the snow fraction described in Section 2.3 is estimated based on two main sources of error:

1. Angle of the field of view (FOV): defined the circular area of the image pixels that were selected for processing;
2. The subdomain size d specified in the adaptive thresholding method described in Appendix C.

When the FOV size mentioned gets too large, pixels affected by the vignette effect and beyond correction is included, which will bias the results. When the FOV size gets too small, we would lose the variation of the snow fraction due to a relative small area. To use as many pixels as possible while avoiding to include contaminated pixels due to vignette effect at the corners, we found the best FOV angle to be 70°. In addition, changing the subdomain size d would slightly change the results. Thus, we obtained 5 sets of snow fraction estimates using FOV angle of 60°, 70°, 80° and a subdomain size d of 1401, 1501, and 1601. Fig. A3 shows the 5 sets of snow fractions estimated from nadir camera images using before-mentioned FOV angles and subdomain sizes. The standard deviation of the 5 sets of snow fraction is used as the uncertainties for the snow fraction for each data point.

3). Radiative transfer calculations

The uncertainty of the radiative transfer (RT) calculations for the "0911-above-cloud" was estimated through the two-stream approximation of the reflectance R

$$R = \frac{\tau+\alpha\cdot(\frac{2\mu}{1-g})}{\tau+(\frac{2\mu}{1-g})} \tag{A6}$$

where τ is the cloud optical thickness, α is the surface albedo, μ is the cosine of the solar zenith angle, and g is the asymmetry parameter. The value of 0.85 is assume for g. In addition, we assume that the two main sources for the uncertainty are from the cloud optical thickness τ and surface albedo α. The uncertainty of R due to the change of τ and α is therefore

$$u(R) = \sqrt{\left(\frac{\partial R}{\partial \tau}u(\tau)\right)^2 + \left(\frac{\partial R}{\partial \alpha}u(\alpha)\right)^2} \tag{A7}$$

This analytical formula allows to calculate uncertainties without numeric radiative transfer calculations.

E. Atmospheric correction

The following steps describe the atmospheric correction applied to the flight level albedo measured by SSFR-BBR.

1) The spectral flight level albedo from SSFR-BBR (referred to as x_0) was scaled by 0.6, 0.7, 0.8, 0.9, and 1.0 (referred to as y_1, y_2, y_3, y_4, and y_5) – each of these are spectra;
2) Five sets of downwelling and upwelling irradiances were obtained from the RTM by changing surface albedo to y_1, y_2, y_3, y_4, and y_5 while keeping the other model inputs the same;
3) From the five sets of downwelling and upwelling irradiances calculated at flight altitude, we can derive five corresponding flight level albedo x_1, x_2, x_3, x_4, and x_5 using Equation (4);
4) The five pairs of $\{x, y\}$ provide a relationship between surface albedo and flight level albedo (nearly linear), $y = ax + b$;
5) The linear relationship was inverted to infer the surface albedo spectrum from the measurements at flight level ($ax_0 + b$).

The atmospheric correction corrected less than 0.2% on flight level albedo at the non-absorbing wavelengths.

F. Extending spectral surface albedo

To obtain the spectral surface albedo for a wavelength range from 200 nm to 3600 nm, several techniques were performed. Using the spectral surface albedo for "0911-above-cloud" (Fig. 6) as an example, the following steps were followed:

1) The spectral surface albedo was calculated from equation (5), e.g., with *SF*=76.4% (marked in red in Fig. 6);
2) In the gas absorption bands (red area in Fig. 6), the surface albedo was replaced with interpolated values;

3) From 1800nm to 1900nm (yellow area in Fig. 6), a polynomial fit was used for extrapolation, based on the spectral dependence from 1650 nm to 1800 nm;
4) For the wavelengths shorter than 350 nm and greater than 1900 nm (green area in Fig. 6), a modeled snow albedo (Wiscombe and Warren, 1981) was used, multiplied with a scale factor to match the measurements at the joinder wavelengths.

5

Acknowledgements. This work was supported by NASA grants NNX12AC11G (SSFR data collection during ARISE) and NNX14AP72G (data analysis). MODIS data were provided by the NASA/Goddard Space Flight Center's Level-1 and Atmosphere Archive and Distribution System (LAADS) (http://dx.doi.org/10.5067/MODIS/MOD06_L2.061).

References

Anderson, G. P., Clough, S. A., Kneizys, F. X., Chetwynd, J. H., and Shettle, E. P.: AFGL atmospheric constituent profiles (0 - 120km). Tech. Rep. AFGL-TR-86–0110, (954), 46, 1986.

Badosa, J., Wood, J., Blanc, P., Long, C. N., Vuilleumier, L., Demengel, D., and Haeffelin, M.: Solar irradiances measured using SPN1 radiometers: Uncertainties and clues for development, Atmos. Meas. Tech., 7(12), 4267–4283, doi:10.5194/amt-7-4267-2014, 2014.

Bannehr, L., and Schwiesow, R.: A technique to account for the misalignment of pyranometers installed on aircraft, J. Atmos. Ocean. Tech., 10, 774–777, 1993.

Bennartz, R., Shupe, M. D., Turner, D. D., Walden, V. P., Steffen, K., Cox, C. J., Kulie, . S., Miller, N.B., and Pettersen, C.: July 2012 Greenland melt extent enhanced by low-level liquid clouds. Nature, 496, 83–86, 2013.

Boggs, P. T. and Rogers J. E.: Orthogonal distance regression. Contemporary Mathematics, 112, 183-94, 1990.

Bosilovich, M., Akella, S., Coy, L., Cullather, R., Draper, C., Gelaro, R., Kovach, R., Liu, Q., Molod, A., Norris, P., Wargan, K., Chao, W., Reichle, R., Takacs, L., Vikhliaev, Y., Bloom, S., Collow, A., Firth, S., Labow, G., Partyka, G., Pawson, S., Reale, O., Schubert, S. D., and Suarez, M: MERRA-2: Initial evaluation of the climate. NASA Tech. Rep. Series on Global Modeling and Data Assimilation NASA/TM-2015-104606, 2015

Brandt, R. E., Warren, S. G., Worby, A. P., and Grenfell, T. C.: Surface albedo of the Antarctic sea ice zone, J. Climate, 18, 3606–3622, 2005.

Bucholtz, A., Bluth, R. T., Kelly, B., Taylor, S., Batson, K., Sarto, A. W., Tooman, T P., and McCoy, Jr., R. F.: The Stabilized Radiometer Platform (STRAP) - An actively stabilized horizontally level platform for improved aircraft irradiance measurements, J. Atmos. Ocean. Tech, 25, 2161–2175, 2008.

Bucholtz, A., Hlavka, D. L., McGill, M. J., Schmidt, K. S., Pilewskie, P., Davis, S. M., Reid, E. A., and Walker, A. L.: Directly Measured Heating Rates of a Tropical Subvisible Cirrus Cloud, J. of Geophys. Res., 115, 1-11, 2010.

Curry, J. A., Schramm, J. L., Serreze, M. C., and Ebert, E. E.: Water vapor feedback over the Arctic Ocean, J. Geophys. Res., 100, 14223–14229, 1995.

Curry, J. A., Rossow, W. B., Randall, D., and Schramm, J. L.: Overview of arctic cloud and radiation characteristics, J. Climate, 9, 1731–1764, 1996.

Davies, E. R.: Machine Vision: Theory, Algorithms, Practicalities, 3rd Edition, Elsevier, Inc., 934 pp., 2005.

Emde, C., Buras-Schnell, R., Kylling, A., Mayer, B., Gasteiger, J., Hamann, U., Kylling, J., Richter, B., Pause, C., Dowling. T. and Bugliaro, L.: The libRadtran software package for radiative transfer calculations (version 2.0.1), Geosci. Model Develop., 9, 1647–1672, doi:10.5194/gmd-9-1647-2016, 2016.

Gardner, A. S., and Sharp, M. J.: A review of snow and ice albedo and the development of a new physically based broadband albedo parameterization. J. Geophys. Res., 115, F01009, doi:10.1029/2009JF001444, 2010.

Gonzalez, R. C., Woods, R. E., and Eddins, S. L.: Image Segmentation. Digital Image Processing, 600–603, 2002.

Haeberli, P., and Voorhies, D.: Image processing by linear interpolation and extrapolation, IRIS Universe Magazine, 28, 8–9, 1994.

Hartmann, D. L., and Ceppi, P.: Trends in the CERES dataset, 2000-13: The effects of sea ice and jet shifts and comparison to

climate models, J. Climate, 27, 2444–2456, 2014.

Henderson, D. S., L'Ecuyer, T., Stephens, G., Partain, P., and Sekiguchi, M.: A multisensor perspective on the radiative impacts of clouds and aerosols, J. Appl. Meteorol. Clim., 52, 853–871, 2013.

Kay, J. E., and L'Ecuyer, T.: Observational constraints on Arctic Ocean clouds and radiative fluxes during the early 21st century, J. Geophys. Res., 118, 7219–7236, 2013.

Kindel, B. C.: Cloud shortwave spectral radiative properties: Airborne hyperspectral measurements and modeling of irradiance, Ph.D. Dissertation, University of Colorado Boulder, United States, 130 pp., 2010.

King, M. D., Platnick, S., Yang, P., Arnold, G. T., Gray, M. A., Riedi, J. C., Ackerman, S. A., and Liou, K. N.: Remote sensing of liquid water and ice cloud optical thickness and effective radius in the Arctic: Application of airborne multispectral MAS data, J. Atmos. Ocean. Tech, 21, 857–875, 2004.

Kurucz, R. L.: Synthetic infrared spectra, In Infrared Solar Physics, Rabin, D. M., Jefferies, J. T., and Lindsey, C. (Eds.), Springer-Science+Business Media, B. V., 523–531, 1992.

Lyapustin, A., Gatebe, C. K., Kahn, R., Brandt, R., Redemann, J., Russell, P., King, M. D., Pedersen, C. A., Gerland, S., Poudyal, R., Marshak, A., Wang, Y., Schaaf, C., Hall, D., and Kokhanovsky, A.: Analysis of snow bidirectional reflectance from ARCTAS Spring-2008 campaign, Atmos. Chem. Phys., 10, 4359–4375, 2010.

Liu, Y., Ackerman, S. A., Maddux, B. C., Key, J. R., and Frey, R. A.: Errors in cloud detection over the arctic using a satellite imager and implications for observing feedback mechanisms, J. Climate, 23, 1894–1907, 2010.

Loeb, N. G., and Manalo-Smith, N.: Top-of-atmosphere direct radiative effect of aerosols over global oceans from merged CERES and MODIS observations, J. Climate, 18, 3506–3526, 2005.

Loeb, N. G., Kato, S., Su, W., Wong, T., Rose, F. G., Doelling, D. R., Norris, J. R., and Huang, X.: Advances in understanding top-of-atmosphere radiation variability from satellite observations, Surv. Geophys., 33, 359–385, 2012.

Long, C. N., Bucholtz, A., Jonsson, H., Schmid, B., Vogelmann, A., and Wood, J.: A method of correcting for tilt from horizontal in downwelling shortwave irradiance measurements on moving platforms, The Open Atmos. Sci. J., 4, 78–87, 2010.

Malinka, A., Zege, E., Heygster, G., and Istomina, L.: Reflective properties of white sea ice and snow, The Cryosphere, 10, 2541–2557, https://doi.org/10.5194/tc-10-2541- 2016, 2016.

Malinka, A., Zege, E., Istomina, L., Heygster, G., Spreen, G., Perovich, D., and Polashenski, C.: Reflective properties of melt ponds on sea ice, The Cryosphere, 12, 1921–1937, https://doi.org/10.5194/tc-12-1921-2018, 2018.

Moody, E. G., King, M. D., Schaaf, C. B., Hall, D. K., and Platnick, S.: Northern Hemisphere five-year average (2000-2004) spectral albedos of surfaces in the presence of snow: Statistics computed from Terra MODIS land products, Remote Sens. Environ., 111, 337–345, 2007.

Nakajima, T., and King, M. D.: Determination of the optical thickness and effective particle radius of clouds from reflected solar radiation measurements. Part I: Theory, J. Atmos. Sci., 47, 1878–1893, 1990.

Oreopoulos, L., Cho, N., Lee, D., and Kato, S.: Radiative effects of global MODIS cloud regimes, J. Geophys. Res., 121, 2299–2317, 2016.

Perovich, D. K., Tucker, W. B., and Ligett, K. A.: Aerial observations of the evolution of ice surface conditions during summer, J. Geophys. Res., 107, SHE24-1–SHE24-14, https://doi.org/10.1029/2000JC000449, 2002.

Perovich, D. K.: Seasonal evolution of the albedo of multiyear Arctic sea ice, J. Geophys. Res., 107(C10), 8044, doi: 10.1029/2000JC000438, 2002.

Pierluissi, J. H., and Peng, G. : New molecular transmission band models for LOWTRAN, Optical Engineering, 24, 541–547, doi: 10.1117/12.7973523, 1985.

Pilewskie, P., Pommier, J., Bergstrom, R., Gore, W., Howard, S., Rabbette, M., Schmid, B., Hobbs, P. V., and Tsay, S. C.: Solar spectral radiative forcing during the Southern African Regional Science Initiative, J. Geophys. Res., 108(D13), 8486, doi:10.1029/2002JD002411, 2003.

Platnick, S., Li, J. Y., King, M. D., Gerber, H., and Hobbs, P. V.: A solar reflectance method for retrieving the optical thickness and droplet size of liquid water clouds over snow and ice surfaces, J. Geophys. Res., 106, 15185–15199, 2001.

Platnick, S., King, M. D., Ackerman, S. A., Menzel, W. P., Baum, B. A., Riédi, J. C., and Frey, R. A.: The MODIS cloud products: Algorithms and examples from Terra, IEEE Trans. Geosci. Remote Sens., 41, 459–473, 2003.

Platnick, S., Ackerman, S. A., King, M. D., Wind, G., Meyer, K., Menzel, W. P., Frey, R. A., Holz, R. E., Baum, B. A., and Yang, P.: MODIS Atmosphere L2 Cloud Product (06_L2). NASA MODIS Adaptive Processing System, Goddard Space Flight Center, USA, http://dx.doi.org/10.5067/MODIS/MOD06_L2.006, 2017.

Platnick, S., Meyer, K. G., King, M. D., Wind, G., Amarasinghe, N., Marchant, B., Arnold, G. T., Zhang, Z., Hubanks, P. A., Holz, R. E., and Yang, P.: The MODIS cloud optical and microphysical products: Collection 6 updates and examples from Terra and Aqua, IEEE Trans. Geosci. Remote Sens., 55, 502-525, 2017.

Platnick, S., Meyer, K. G., King, M. D., Wind, G., Amarasinghe, N., Marchant, B., Arnold, G. T., Zhang, Z., Hubanks, P. A., Ridgway, B., and Riedi, J.: MODIS Cloud Optical Properties: User Guide for the Collection 6/6.1 Level-2 MOD06/MYD06 Product and Associated Level-3 Datasets version 1.1, https://atmosphere-imager.gsfc.nasa.gov/sites/default/files/ModAtmo/MODISCloudOpticalPropertyUserGuideFinal_v1.1.pdf, 2018.

Rozenhaimer, M., Barton, N., Redemann, J., Schmidt, S., LeBlanc, S., Anderson, B., Winstead, E., Corr, C. A., Moore, R., Thornhill, K. L., and Cullather, R. I.: Bias and sensitivity of boundary layer clouds and surface radiative fluxes in MERRA-2 and airborne observations over the Beaufort Sea during the ARISE campaign, J. Geophs. Res. Atmos., 123, doi: 10.1029/2018JD028349.

Schmidt, S., Pilewskie, P., Mayer, B., Wendisch, M., Kindel, B., Platnick, S., King, M. D., Wind, G., Arnold, G. T., Tian, L., Heymsfield, G., and Kalesse, H.: Apparent absorption of solar spectral irradiance in heterogeneous ice clouds, J. Geophys. Res., 115, D00J22, doi:10.1029/2009JD013124, 2010.

Schmidt, S., and Pilewskie, P.: Airborne measurements of spectral shortwave radiation in cloud and aerosol remote sensing and energy budget studies, In A. A. Kokhanovsky (Ed.), Light Scattering Reviews, Vol. 6: Light Scattering and Remote Sensing of Atmosphere and Surface, Berlin, Heidelberg: Springer Berlin Heidelberg, 239–288, doi:10.1007/978-3-642-15531-4_6, 2012.

Shupe, M. D., Walden, V. P., Eloranta, E., Uttal, T., Campbell, J. R., Starkweather, S. M., and Shiobara, M.: Clouds at Arctic atmospheric observatories. Part I: Occurrence and macrophysical properties, J. Appl. Meteorol. Clim., 50, 626–644, 2011.

Shupe, M. D., and Intrieri, J. M.: Cloud radiative forcing of the Arctic surface: The influence of cloud properties, surface albedo, and solar zenith angle, J. Climate, 17, 616–628, 2004.

Smith, W. L., Hansen, C., Bucholtz, A., Anderson, B. E., Beckley, M., Corbett, J. G., Cullather, R. I., Hines, K.M., Hofton, M., Kato, S., Lubin, D., Moore, R. H., Segal Rosenhaimer, M., Redemann, J., Schmidt, S., Scott, R., Song, S., Barrick, J. D., Blair, J.B., Bromwich, D. H., Brooks, C., Chen, G., Cornejo, H., Corr, C. A., Ham, S., Kittelman, A. S., Knappmiller, S., LeBlanc, S., Loeb, N. G., Miller, C., Nguyen, L., Palikonda, R., Rabine, D., Reid, E. A., Richter-Menge, J. A., Pilewskie, P., Shinozuka, Y., Spangenberg, D., Stackhouse, P., Taylor, P., Thornhill, K. L., van Gilst, D., and Winstead, E.: Arctic Radiation-IceBridge Sea and Ice Experiment: The Arctic radiant energy system during the critical seasonal ice transition. Bull. Amer. Meteor. Soc., 98, 1399–1426, https://doi.org/10.1175/BAMS-D-14-00277.1, 2017

Stamnes, K., Tsay, S.-C., Wiscombe, W., and Jayaweera, K.: Numerically stable algorithm for discrete-ordinate-method radiative

transfer in multiple scattering and emitting layered media, Appl. Opt., 27, 2502–2509, 1988.

Strahler, A. H., Lucht, W., Schaaf, C. B., Tsang, T., Gao, F., Li, X., Muller, J., Lewis, P., and Barnsley, M. J.: MODIS BRDF/albedo product: algorithm theoretical basis document version 5.0, https://lpdaac.usgs.gov/documents/97/MCD43_ATBD.pdf, 1999.

Warren, S. G., Roesler, C. S., and Brandt, R. E.: Solar radiation processes in the east Antarctic sea-ice zone. Antarctic J. United States, 32, 185–186, 1997.

Wendisch, M., Müller, D., Schell, D., and Heintzenberg, J.: An airborne spectral albedo meter with active horizontal stabilization, J. Atmos. Ocean. Tech, 18, 1856–1866, 2001.

Wielicki, B. A., Barkstrom, B. R., Harrison, E. F., Lee III, R. B., Smith, G. L., and Cooper, J. E.: Clouds and the Earth's Radiant Energy System (CERES): An Earth Observing System Experiment. Bull. Amer. Meteor. Soc., 77, 853–868, 1996.

Wiscombe, W. J., and Warren, S. G.: A model for the spectral albedo of snow. I: Pure snow, J. Atmos. Sci., 37, 2712–2733, 1981.

11 September

13 September

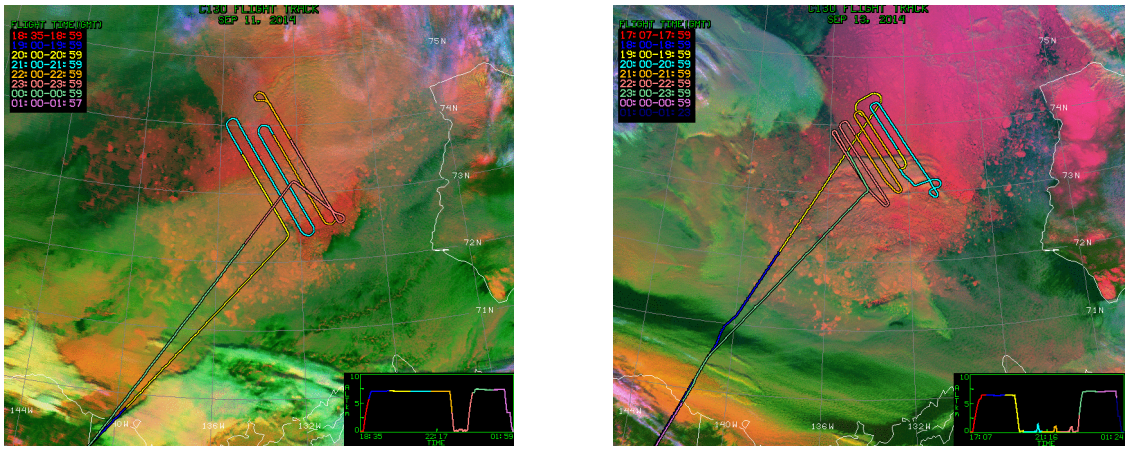

Figure 1. ARISE flight tracks overlaid on MODIS false color imagery (0.65 μm for red, 11 μm for blue, and 3.7-11 μm for green) from NASA Langley Research Center on 11 September and 13 September 2014. The focus region if these two research flights was [136W, 130W, 72.5N, 74.5N] in the marginal ice zone.

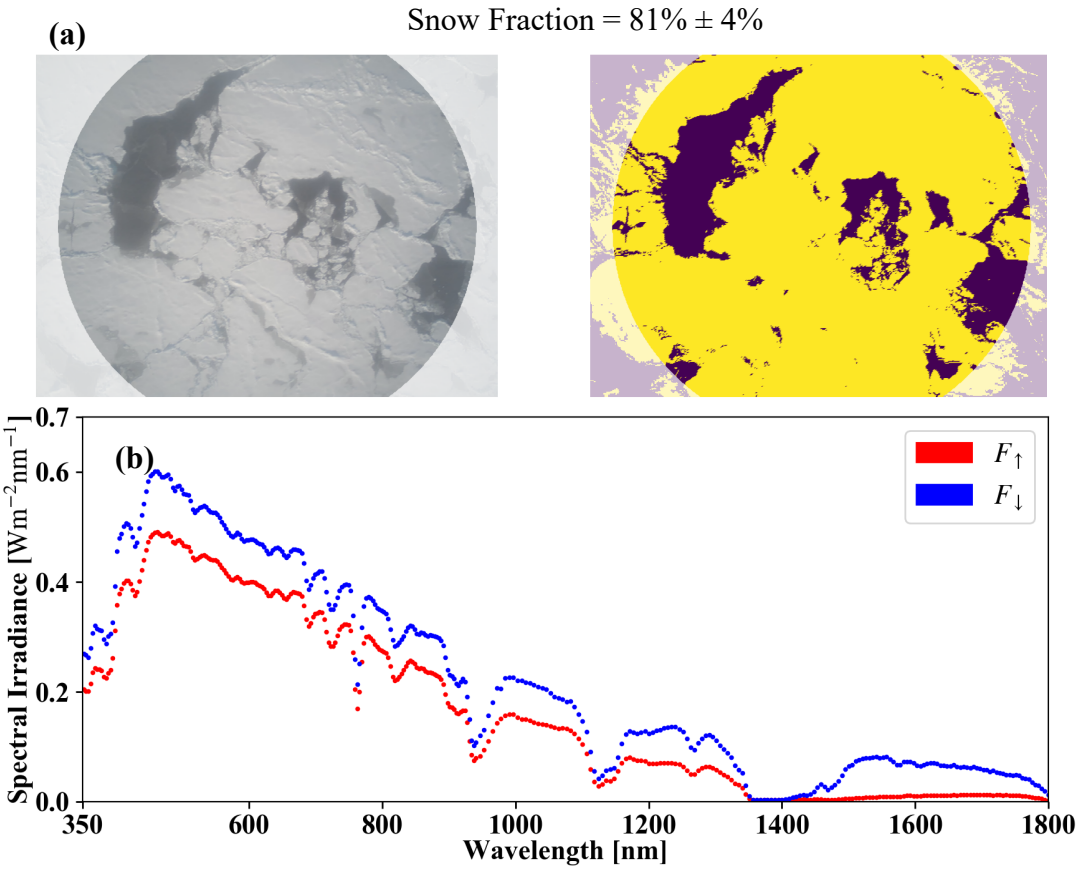

Figure 2. **(a)** An example of the snow fraction along with its uncertainty estimated from the nadir camera imagery at 20:03:32 UTC on 13 September, at a location of (-132.95º, 73.85º). The flight altitude was 134 m. The left panel is the nadir camera imagery. The diameter of the field of view was about 380 m. The right panel uses yellow and purple to indicate bright and dark pixels as detected by the adaptive thresholding method. The snow fraction is derived from the abundance of yellow pixels. **(b)** The upwelling and downwelling irradiance from SSFR-BBR at the same time.

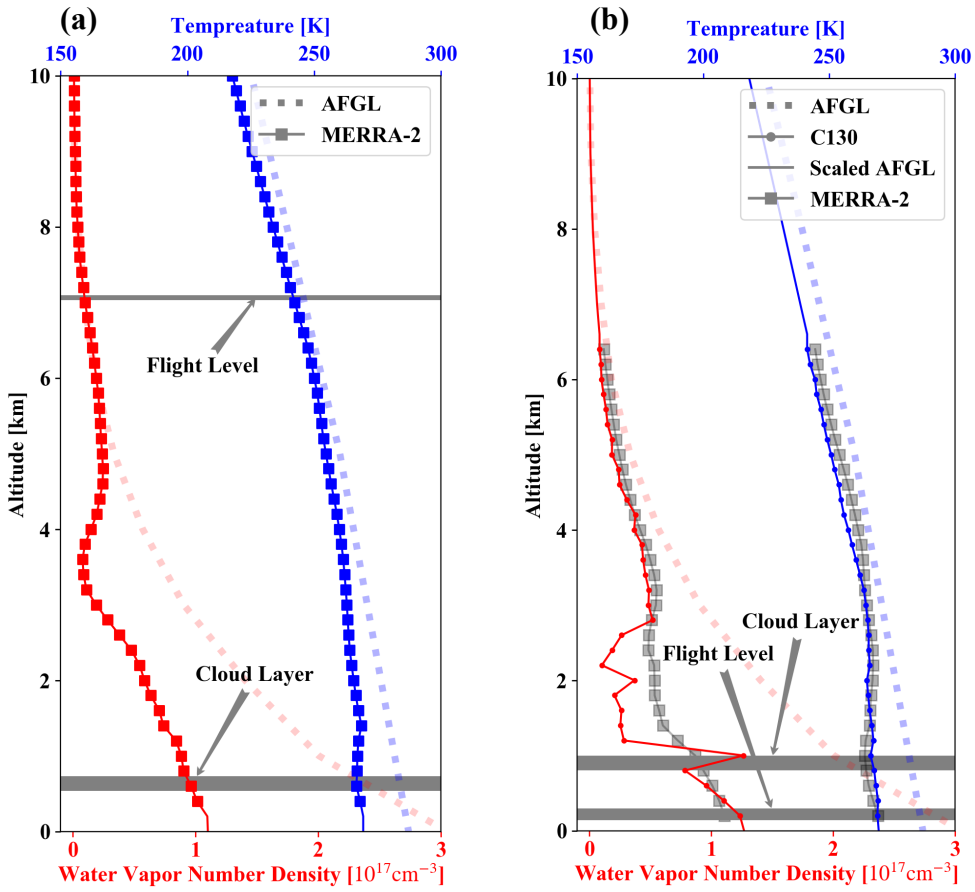

Figure 3. Vertical profiles of temperature and water vapor from MERRA-2 and from the climatology (AFGL) for (a) 11 September and (b) from the C130 for 13 September 2014. On 11 September, MERRA-2 data at 21:00 UTC was averaged over the region of [135W, 130.625W, 72.5N, 74N] to represent the atmospheric profile there. The vertical cloud distribution was unavailable from the in-situ data. On 13 September, aircraft data from a descending leg (19:31 UTC to 19:50 UTC at 133.8W, 74.1N) was used for the atmospheric profiles. Based on the water vapor profile, the cloud was likely located below 1.0 km (indicated in grey). Since hygrometer measurements were not available on 11 September, the cloud top height (1.1 km) was obtained from the MODIS L2 product), and the geometric thickness was set to 0.2 km (just like on September 13). The flight level range is also shown. The solid lines for both days represent the temperature and water vapor profiles that went into the radiative transfer calculations.

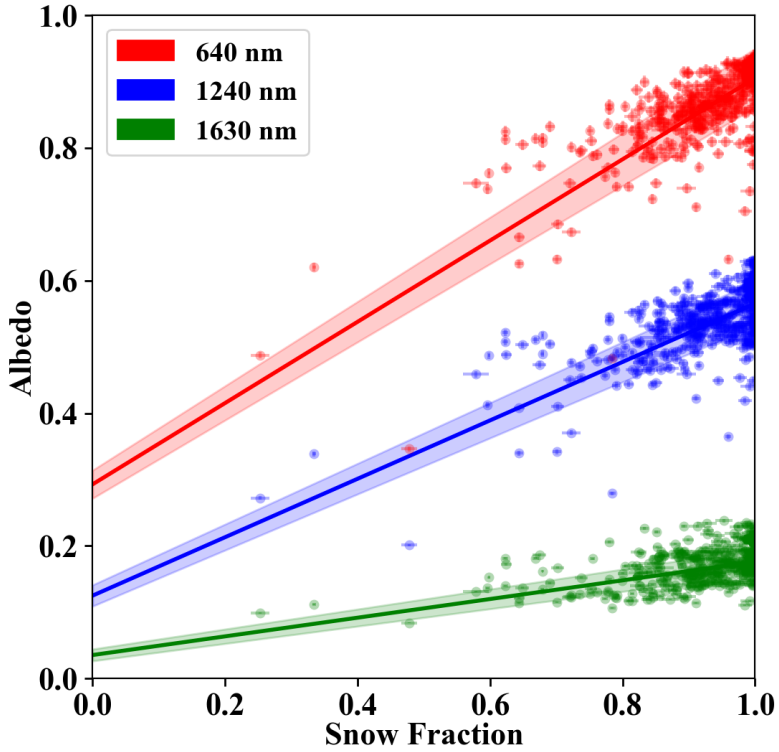

Figure 4. Estimated snow fraction from nadir imagery versus SSFR-BBR measured surface albedo at 640 nm, 1240 nm, and 1630 nm. The surface albedo and snow fraction uncertainties are indicated as vertical and horizontal error bars. The solid lines show linear regression fits, and the shaded region indicates their uncertainties.

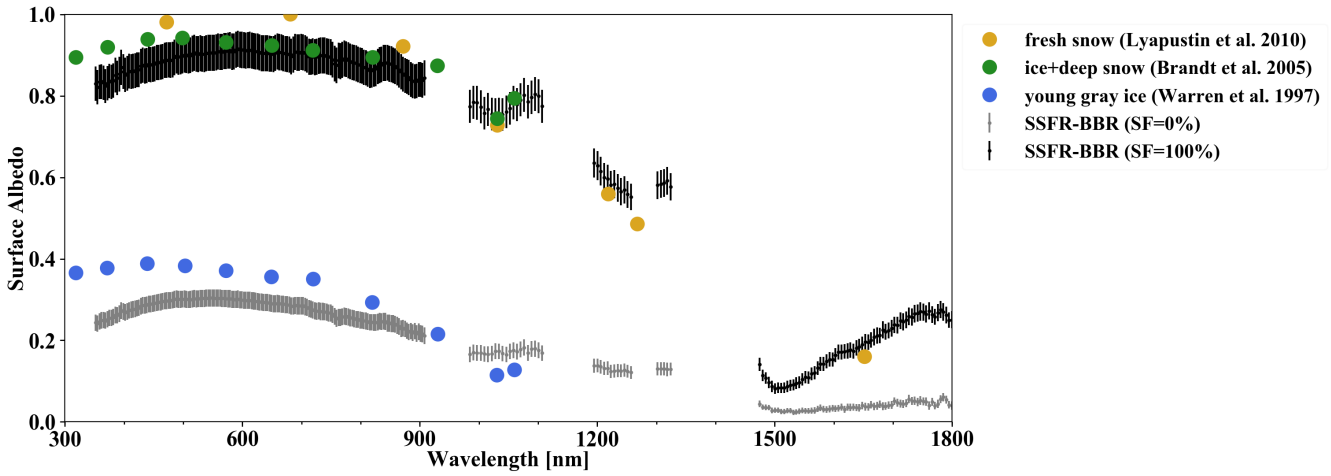

Figure 5: Spectral surface albedo derived from SSFR-BBR measurements for *SF*=100% (black) and *SF*=0 (gray), along with their uncertainties. In addition, different albedos from the literature are shown for comparison.

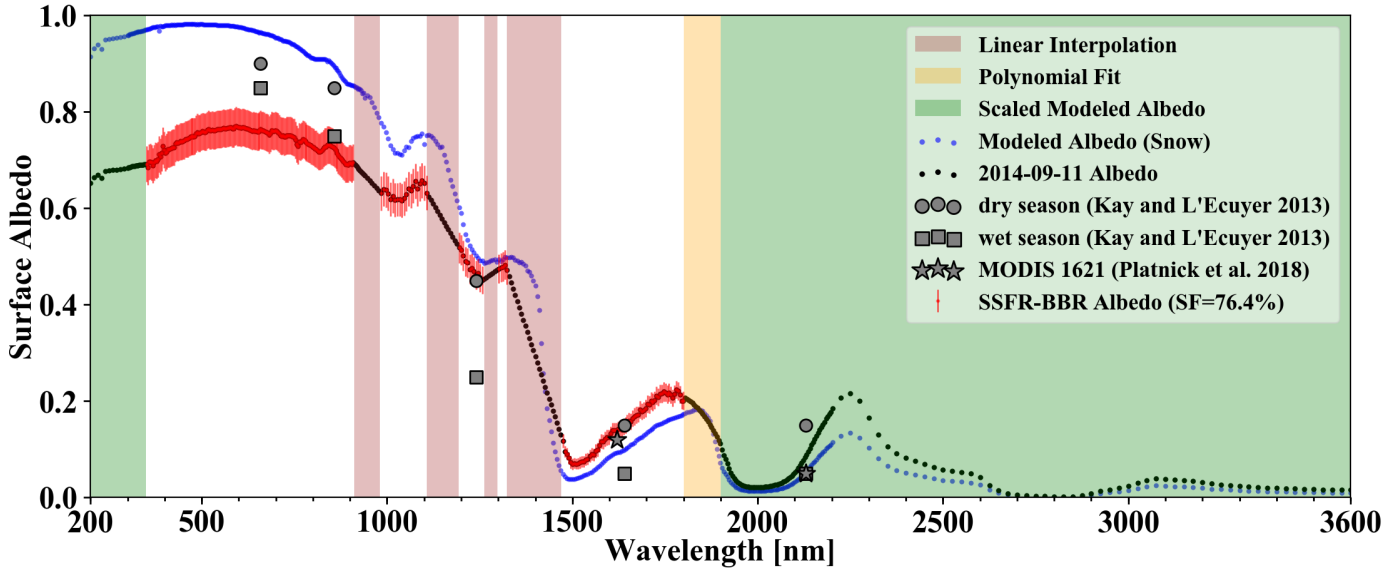

Figure 6: Spectral surface albedo (black) along with their uncertainties used in the RTM for the 2014-09-11 calculations. The spectral albedo uses the SSFR-BBR derived albedo with *SF*=76.4% (red) except for the wavelength ranges marked (1) in green: replaced by scaled modeled snow albedo (blue); (2) in red (gas absorption bands): linear interpolation; and (3) in yellow (1800nm to 1900nm): polynomial fit using SSFR-BBR derived albedo from 1650nm to 1800nm.

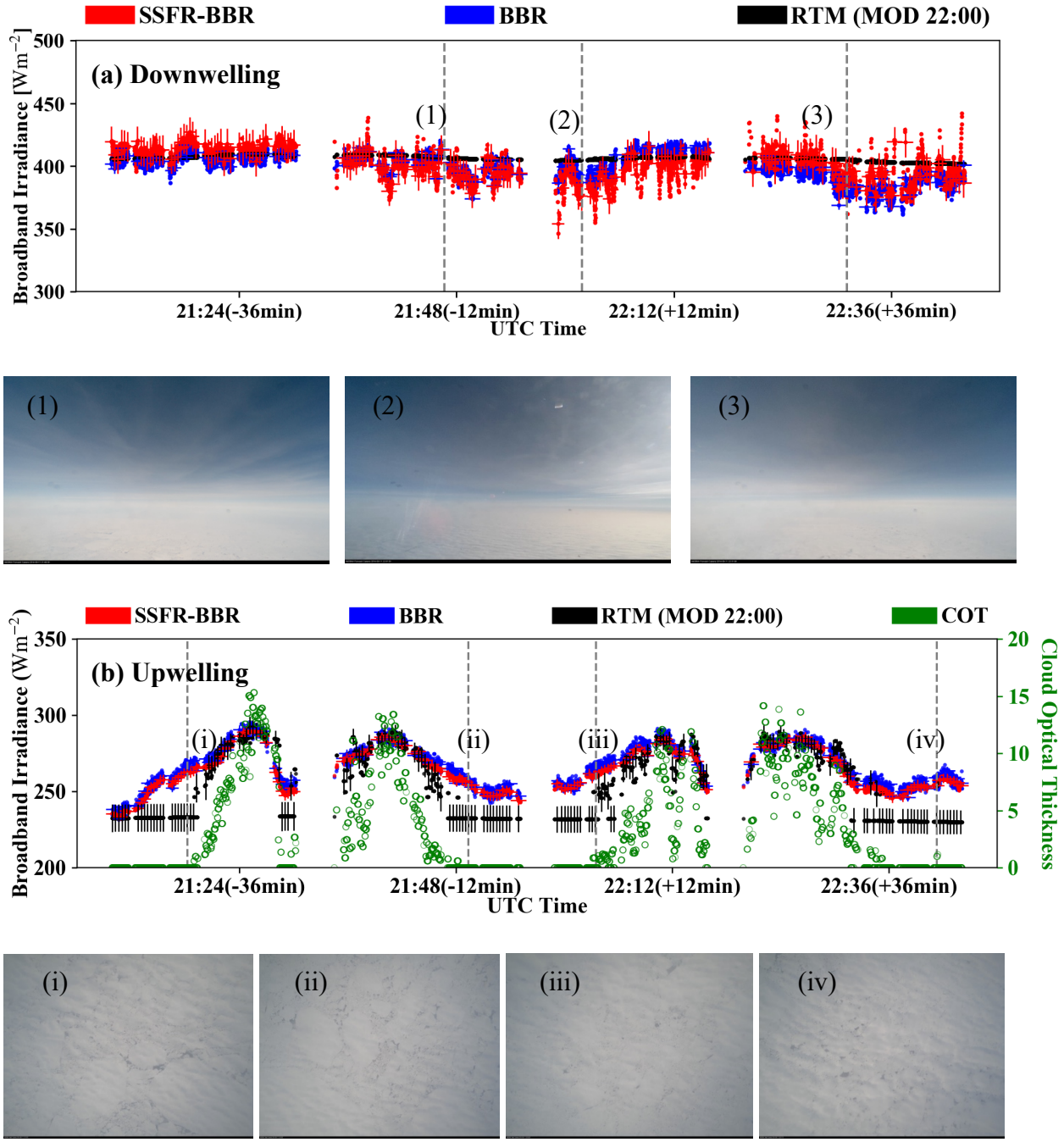

Figure 7. Broadband (a) downwelling and (b) upwelling irradiance from SSFR-BBR, BBR, and MODIS-COPs (Terra MODIS at 22:00) based RTM calculations on 11 September (above-clouds) along with their uncertainties. The observed irradiances include a horizontal error bar (indicating the size of the SSFR-BBR FOV) in addition to the vertical error bar (indicating the uncertainty of SSFR-BBR irradiance). The cloud optical thickness from MODIS is indicated in green. The average cloud optical thinness is 6.03. The forward camera images are provided at (1) 21:46:39, (2) 22:01:53, and (3) 22:31:05. The nadir camera images are provided at (i) 21:18:15, (ii) 21:49:22, (iii) 22:03:28, and (iv) 22:41:18 UTC. The time differences between aircraft measurements and MODIS granule are indicated in the axis labels. The average flight altitude was 7 km and the average aircraft ground speed was 150 m/s.

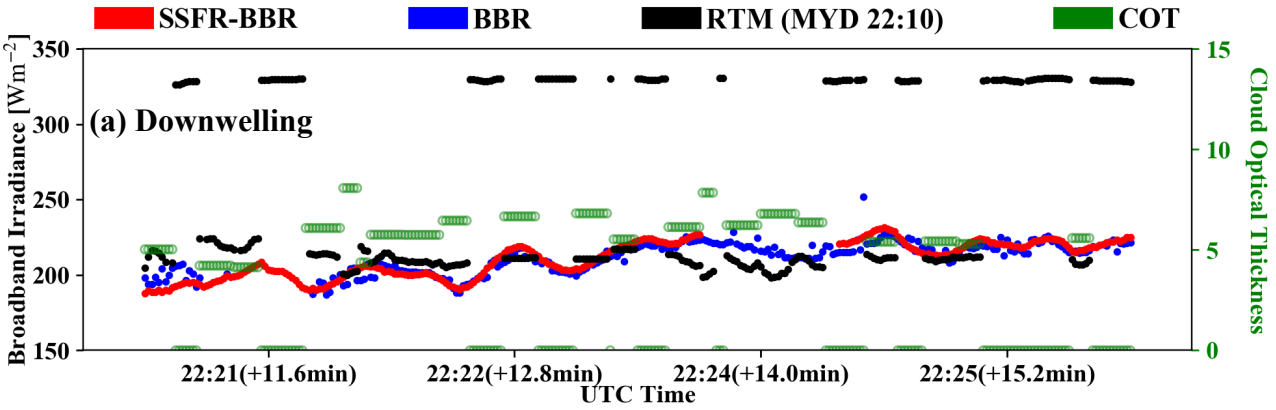
SSFR-BBR
BBR
RTM (MYD 22:10)
COT
(a) Downwelling
Broadband Irradiance [Wm^{-2}]
Cloud Optical Thickness
350
300
250
200
150
15
10
5
0
22:21(+11.6min)
22:22(+12.8min)
22:24(+14.0min)
22:25(+15.2min)
UTC Time

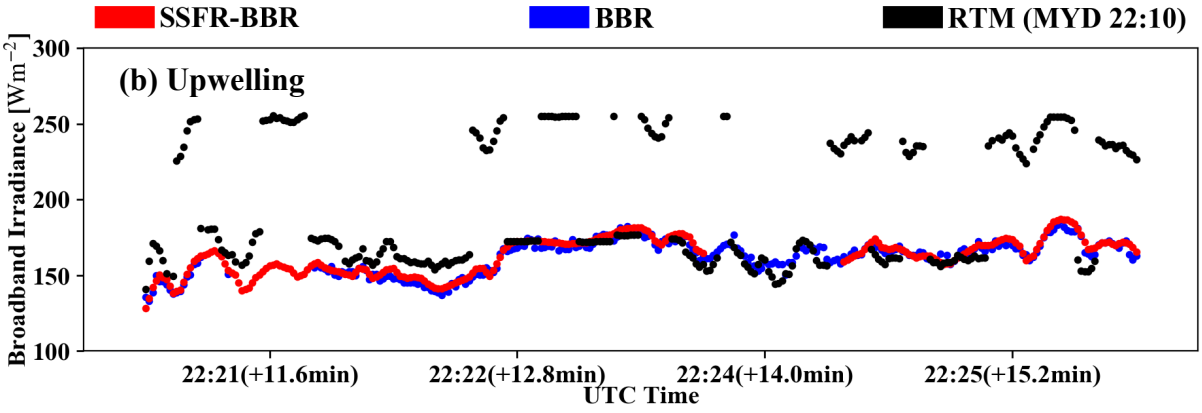
SSFR-BBR
BBR
RTM (MYD 22:10)
(b) Upwelling
Broadband Irradiance [Wm^{-2}]
300
250
200
150
100
22:21(+11.6min)
22:22(+12.8min)
22:24(+14.0min)
22:25(+15.2min)
UTC Time

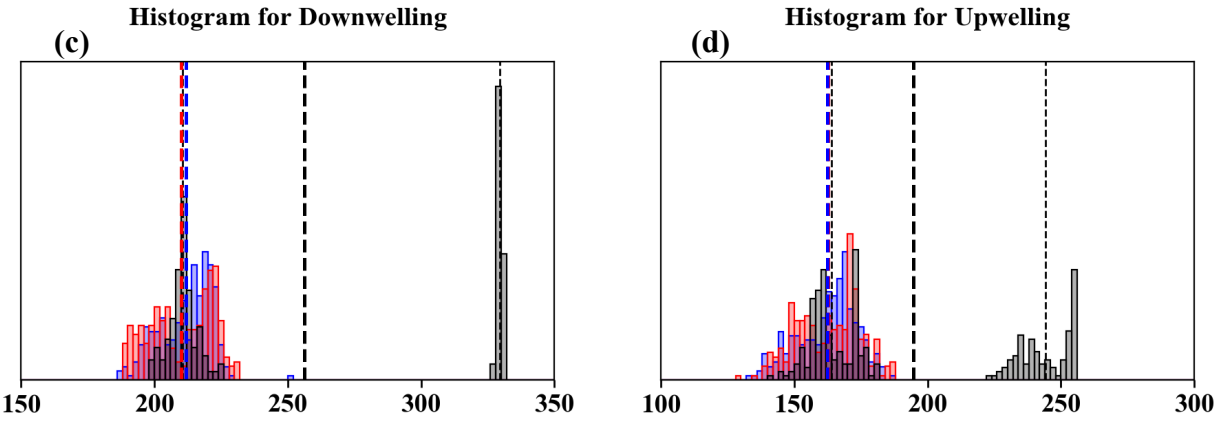
Histogram for Downwelling
(c)
150
200
250
300
350
Histogram for Upwelling
(d)
100
150
200
250
300

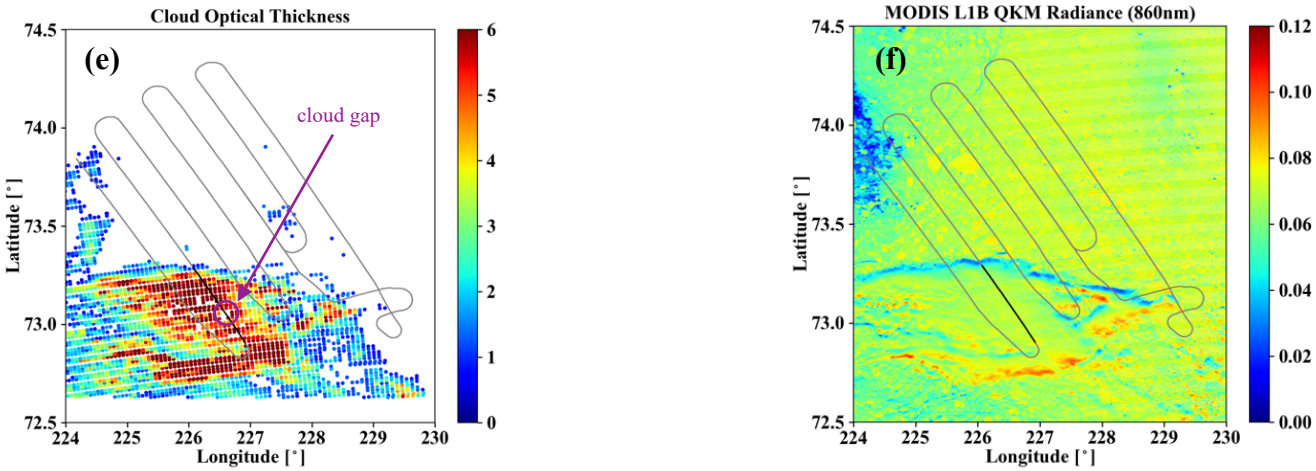

Figure 8. Broadband (a) downwelling and (b) upwelling irradiance from SSFR-BBR, BBR, and MODIS-COPs (Aqua MODIS at 22:10) based RTM calculations on 13 September (below-clouds) and (c) and (d) the histograms. The time difference between aircraft measurements and MODIS granule is indicated in the axis labels. In the histograms, the mean of BBR, SSFR-BBR, and RTM calculations are indicated by the thick dashed lines. The mean is calculated for each of the two modes in RTM calculations and indicated by the thin dashed lines. In addition, the field of cloud optical thickness and radiance at 860 nm from MODIS are provided in (e) and (f). On the map, the black line indicates the flight track studied in (a) – (d). The average flight altitude was 235 m, and the average aircraft ground speed was 106 m/s.

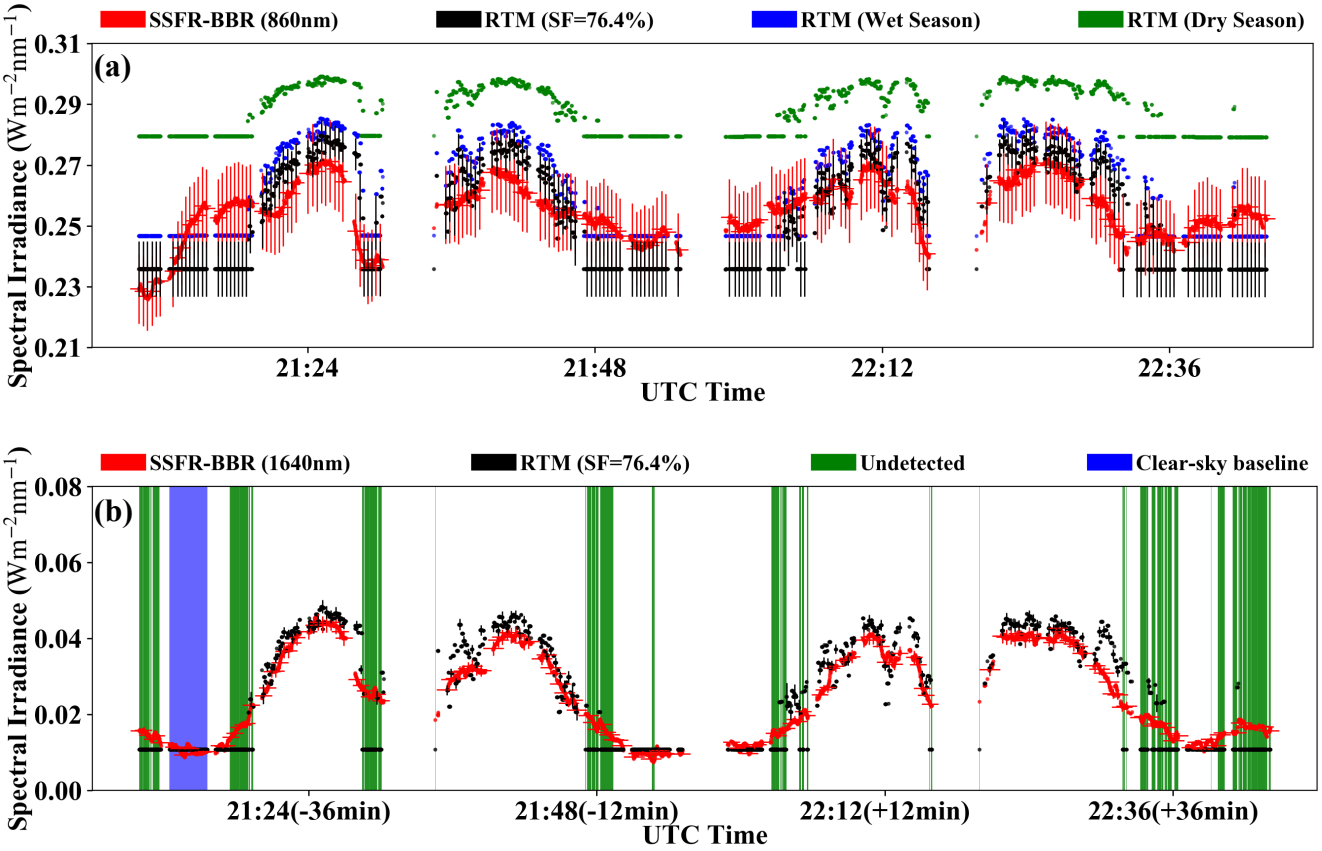

Figure 9. Spectral upwelling irradiance at 860nm (panel a) and 1640nm (panel b) from SSFR-BBR (red) and MODIS-COPs based RTM calculations using "13 September surface albedo" with *SF*=76.4% (black) on 11 September. In addition, calculations with climatological snow albedos are shown in panel (a) (Arctic wet season: 0.75; Arctic dry season: 0.85). The time periods where clouds were not detected are marked in green in panel (b). The clear-sky period that was used to determine the snow fraction is highlighted in blue in panel (b). The uncertainties of the spectral irradiances are indicated as vertical error bars, and the horizontal error bars correspond to the radiometer FOV as in Figure 7. Both need to be considered to identify undetected clouds.

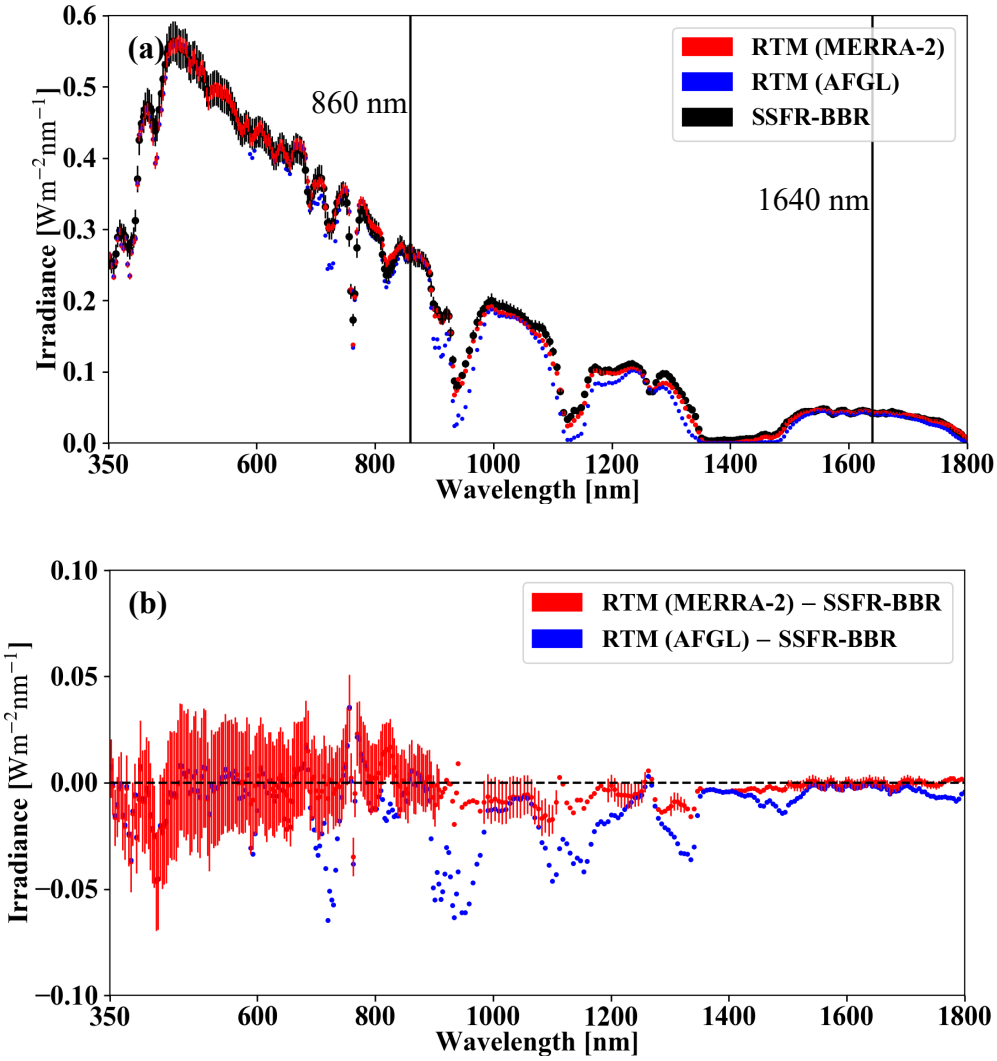

Figure 10. (a) Spectral upwelling irradiance from SSFR-BBR (black) and MODIS-COPs based RTM calculations with atmospheric profiles from MERRA-2 (red) and with AFGL subarctic summer climatology (blue) at 21:24 UTC on 11 September. (b) Irradiance difference between RTM and SSFR-BBR. The uncertainty of the SSFR-BBR irradiance is indicated as error bars (for one spectrum only).

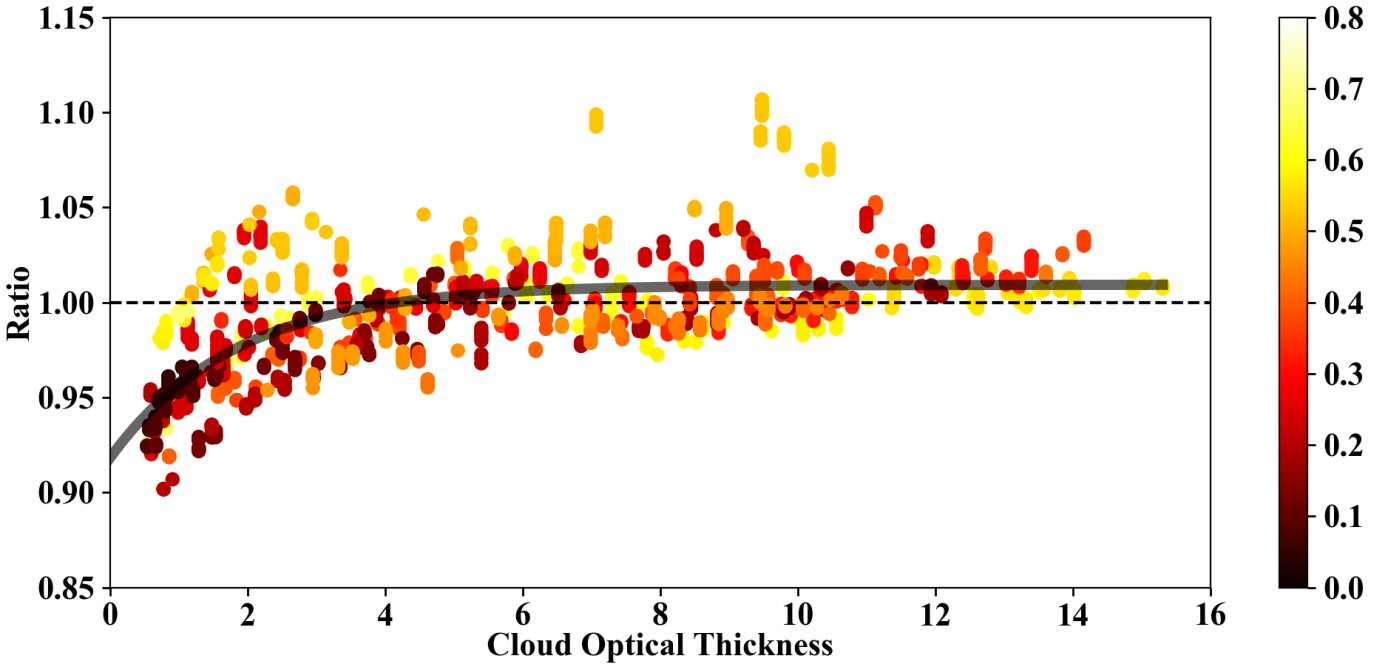

Figure 11. Ratio (RTM/SSFR-BBR) of upwelling broadband irradiance as a function of cloud optical thickness from MODIS "1621" cloud product on 11 September. The time differences between aircraft measurements and MODIS granule (unit: hour) is color-coded. The black curve is an exponentially fitted line using $r = a - e^{b \cdot COT + c}$, where $a = 1.0093$, $b = -0.5464$, and $c = -2.3954$.

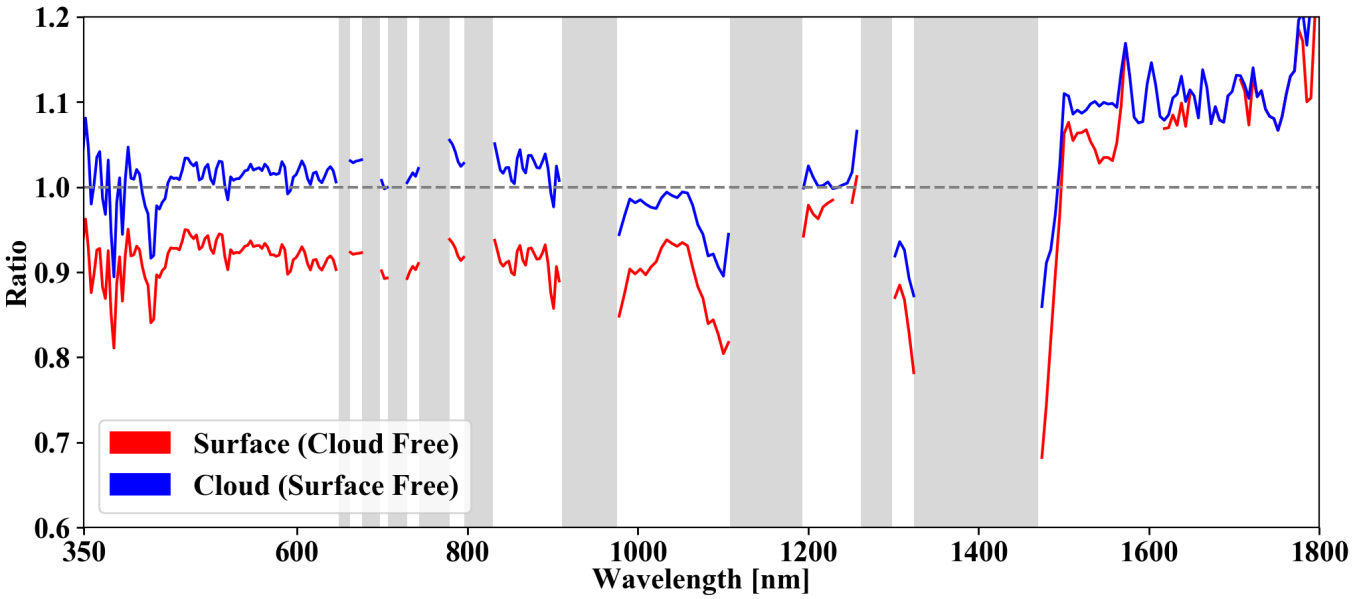

Figure 12. The spectrum of ratio when $COT = 0$ (red, indicating cloud free) and when $COT = \infty$ (blue, indicating surface free) for wavelengths range from 350 nm to 1800 nm. The gas absorption bands are indicated in gray. Ratios at the gas absorption bands are excluded.

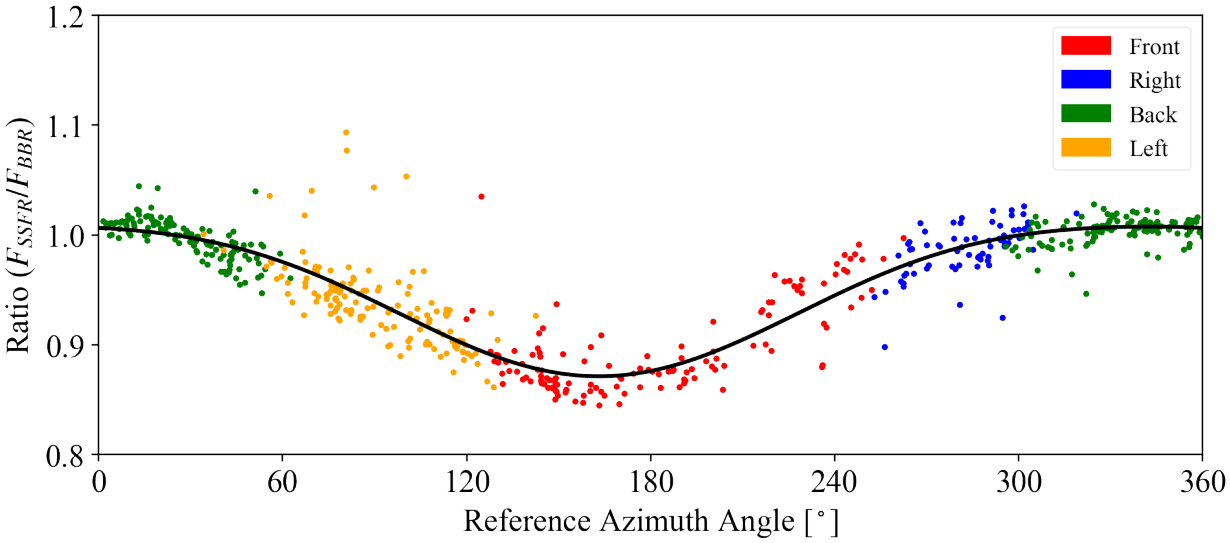

Figure A1: Ratio between spectrally integrated SSFR downwelling irradiance and broadband downwelling irradiance from BBR as a function of reference azimuth angle (solar azimuth position with respect to the sensor, 0 degree pointing north) during 1:00 UTC – 1:36 UTC on 2014-10-03. The relative positions of the sun with respect to the aircraft are indicated by different colors. The black curve is a fitted function using a second order Fourier series.

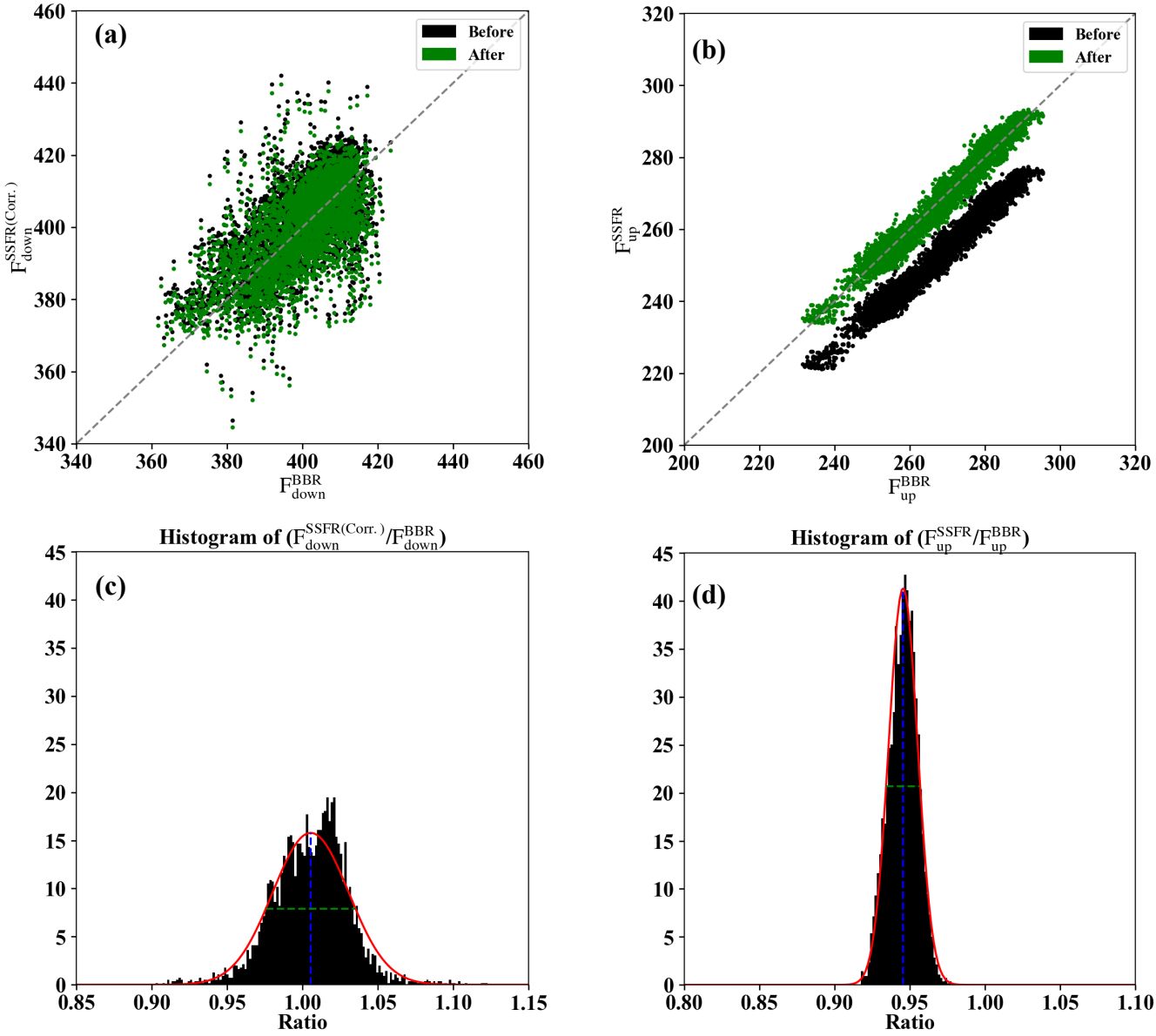

Figure A2: SSFR integrated broadband irradiance versus BBR broadband irradiance (a: downwelling; b: upwelling) and the histograms of the ratio of SSFR integrated broadband irradiance to BBR broadband irradiance (c and d) for the "0911-above-cloud" case. The mean and the full width half maximum of the Gaussian distribution of the ratio are indicated as blue and green dashed lines in the histogram plots. The SSFR-BBR data (SSFR after applying the scale factor as indicated by the blue dashed line) versus BBR is indicated in green in (a) and (b).

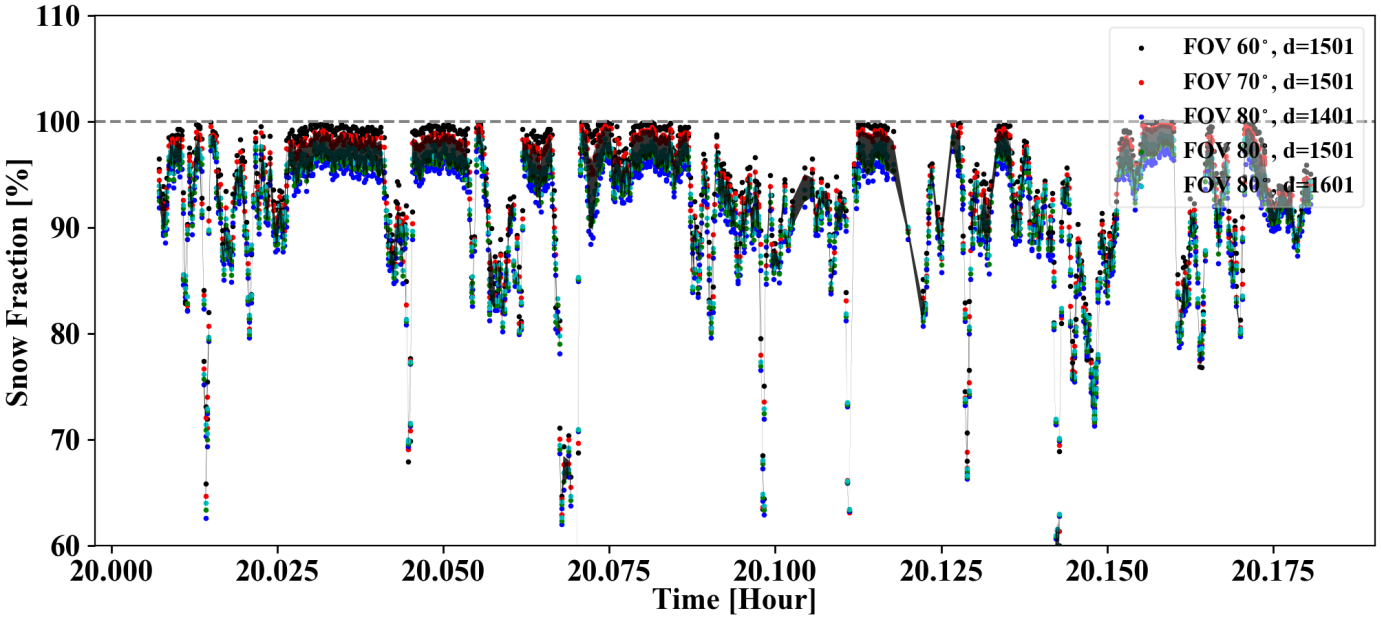

Figure A3: Snow fraction estimated using different FOV angles and subdomain sizes in the adaptive thresholding. The standard deviation of the 5 sets of snow fraction is shaded in black.